

Novel two component dark matter features in the $Z_2 \times Z_2$ 3HDM

Rafael Boto,^{1,*} Pedro N. Figueiredo,^{1,†} Jorge C. Romão,^{1,‡} and João P. Silva^{1,§}

¹*Departamento de Física and CFTP, Instituto Superior Técnico,
Universidade de Lisboa, Av Rovisco Pais, 1, P-1049-001 Lisboa, Portugal*

We discuss the constraints and phenomenology of the $Z_2 \times Z_2$ three Higgs doublet model (3HDM) with two inert scalars, originating two dark matter (DM) particles. We elucidate the competing vacua and we submit the model to all theoretical and current experimental constraints. We find unexplored regions of parameter space and investigate their experimental signatures. In particular, we find regions where the two DM particles contribute equally to the relic DM density.

I. INTRODUCTION

The quest to understand the nature of the elusive dark matter (DM) in the context of a complete model of particle physics persists as one of the paramount challenges in modern physics. It is embarrassing that a very precise Standard Model (SM) has been developed in order to explain around 15% of matter in the Universe, while the 85% DM remains unexplained [1]. On the other hand, the SM postulates that there is one fundamental scalar doublet [2, 3], predicting that there will be a massive neutral scalar particle; the Higgs boson (h). This was confirmed at LHC in 2012 with the discovery of the first neutral scalar at $m_h = 125\text{GeV}$ [4, 5]. But having one single doublet is the simplest, but an otherwise arbitrary imposition. Indeed, the number of scalars (as the number of fermion families a few decades ago) must be determined experimentally. And, the so-called N Higgs doublet models (NHDM) also offer an avenue to solve the DM problem.

In its simplest form, one would add one single scalar doublet to the SM, odd under a Z_2 symmetry that leaves all the SM fields unchanged. If, upon spontaneous symmetry breaking, the new field does not develop a vacuum expectation value, then the Z_2 symmetry remains unbroken and will be reflected in the particle spectrum. The lightest of the Z_2 -odd particles cannot decay and, if it is neutral, it is a candidate for DM; this is the so-called Inert Doublet Model (IDM) [6–9]. There are many interesting articles on the IDM, including, for example [10–13]. The upshot of all theoretical, collider, astrophysical and cosmological constraints is that the DM candidate can only have its mass restricted to two regions; one region around $m_h/2$ and another region with mass above around 500GeV . The exclusion of the intermediate region comes from an interplay between the requirements from relic density and the constraints from direct detection (DD) experiments. In addition, a variety of indirect detection (ID) constraints can arise from DM annihilation into photons [14–16] cosmic rays [17], or neutrinos [18, 19].

The DM (intermediate) mass region can be extended in theories that have more than one DM component [20]; the so-called multi-component DM models [21–23]. This is due to the possibility that the various components contribute to the relic density and also due to the new processes of co-annihilation [24, 25], DM conversion between sectors [26], and/or semi-annihilation [27]. Examples involving exclusively new scalars include models based on Z_4 [28, 29] or $Z_2 \times Z_2$ [30–33]. An interesting feature of multi-component DM models is that they can be used to explain putative anomalies in uncorrelated DM signals which require different DM mass scales. And they may yield signal detectable at the FCC; see for example [34, 35].

In this article, we study a three Higgs doublet model (3HDM), with a $Z_2 \times Z_2$ symmetry, where two scalar doublets are inert. This leads to two separate DM sectors and two natural DM candidates. Whilst in models based on Z_4 [28, 29] the existence of two DM candidates hinges on a suitable choice of masses such that decays of one sector into the other is kinematically forbidden, this is not the case here, where such decays are symmetry forbidden.

*Electronic address: rafael.boto@tecnico.ulisboa.pt

†Electronic address: pedro.m.figueiredo@tecnico.ulisboa.pt

‡Electronic address: jorge.romao@tecnico.ulisboa.pt

§Electronic address: jpsilva@cftp.ist.utl.pt

We introduce the $\mathbb{Z}_2 \times \mathbb{Z}_2$ potential in section II, where we also discuss the bounded from below (BFB) conditions. In sections III and IV, we discuss in detail all possible vacua, and the conditions guaranteeing that the double inert vacuum is indeed the global minimum, improving on the conditions in [33]. In sections V and VI we set up the scan and list all collider, astrophysical and cosmological constraints which we will use in our simulations. This model has a number of interesting processes relevant for DM studies, including DM conversion and co-annihilation, which we discuss in section VII. The results of our scan, and their discussion and implications are presented in section VIII. We outline our conclusions in section IX. For completeness, we include in appendix A the formulas for the scalar masses in the various vacua, while appendix B contains some derivations concerning the minimization of the angular part.

II. THE $\mathbb{Z}_2 \times \mathbb{Z}_2$ POTENTIAL

A. Notation

Consider a three Higgs doublet model (3HDM) with the $\mathbb{Z}_2 \times \mathbb{Z}_2$ symmetry¹

$$\mathbb{Z}_2 : \phi_1 \rightarrow -\phi_1, \quad \phi_2 \rightarrow \phi_2, \quad \phi_3 \rightarrow \phi_3, \quad (1)$$

$$\mathbb{Z}'_2 : \phi_1 \rightarrow \phi_1, \quad \phi_2 \rightarrow -\phi_2, \quad \phi_3 \rightarrow \phi_3. \quad (2)$$

The quadratic part of the potential is

$$V_2 = m_{11}^2 \phi_1^\dagger \phi_1 + m_{22}^2 \phi_2^\dagger \phi_2 + m_{33}^2 \phi_3^\dagger \phi_3, \quad (3)$$

while its quartic part reads [36]

$$\begin{aligned} V_4 = & \lambda_1 (\phi_1^\dagger \phi_1)^2 + \lambda_2 (\phi_2^\dagger \phi_2)^2 + \lambda_3 (\phi_3^\dagger \phi_3)^2 + \lambda_4 (\phi_1^\dagger \phi_1) (\phi_2^\dagger \phi_2) + \lambda_5 (\phi_1^\dagger \phi_1) (\phi_3^\dagger \phi_3) \\ & + \lambda_6 (\phi_2^\dagger \phi_2) (\phi_3^\dagger \phi_3) + \lambda_7 (\phi_1^\dagger \phi_2) (\phi_2^\dagger \phi_1) + \lambda_8 (\phi_1^\dagger \phi_3) (\phi_3^\dagger \phi_1) + \lambda_9 (\phi_2^\dagger \phi_3) (\phi_3^\dagger \phi_2) \\ & + \left[\lambda''_{10} (\phi_1^\dagger \phi_2)^2 + \lambda''_{11} (\phi_1^\dagger \phi_3)^2 + \lambda''_{12} (\phi_2^\dagger \phi_3)^2 + \text{h.c.} \right]. \end{aligned} \quad (4)$$

An alternative notation for the general $\mathbb{Z}_2 \times \mathbb{Z}_2$ symmetric 3HDM potential, used in [33, 37], has the following form [38, 39]:

$$V = V_0 + V_{\mathbb{Z}_2 \times \mathbb{Z}_2}, \quad (5)$$

$$\begin{aligned} V_0 = & -\mu_1^2 (\phi_1^\dagger \phi_1) - \mu_2^2 (\phi_2^\dagger \phi_2) - \mu_3^2 (\phi_3^\dagger \phi_3) + \lambda_{11} (\phi_1^\dagger \phi_1)^2 + \lambda_{22} (\phi_2^\dagger \phi_2)^2 + \lambda_{33} (\phi_3^\dagger \phi_3)^2 \\ & + \lambda_{12} (\phi_1^\dagger \phi_1) (\phi_2^\dagger \phi_2) + \lambda_{23} (\phi_2^\dagger \phi_2) (\phi_3^\dagger \phi_3) + \lambda_{31} (\phi_3^\dagger \phi_3) (\phi_1^\dagger \phi_1) \\ & + \lambda'_{12} (\phi_1^\dagger \phi_2) (\phi_2^\dagger \phi_1) + \lambda'_{23} (\phi_2^\dagger \phi_3) (\phi_3^\dagger \phi_2) + \lambda'_{31} (\phi_3^\dagger \phi_1) (\phi_1^\dagger \phi_3), \end{aligned}$$

$$V_{\mathbb{Z}_2 \times \mathbb{Z}_2} = \lambda_1 (\phi_1^\dagger \phi_2)^2 + \lambda_2 (\phi_2^\dagger \phi_3)^2 + \lambda_3 (\phi_3^\dagger \phi_1)^2 + \text{h.c.}$$

Comparing with Eqs. (3) and (4), the relation between the two notations is

$$-\mu_1^2 \rightarrow m_{11}^2, \quad -\mu_2^2 \rightarrow m_{22}^2, \quad -\mu_3^2 \rightarrow m_{33}^2, \quad (6)$$

$$\lambda_{11} \rightarrow \lambda_1, \quad \lambda_{22} \rightarrow \lambda_2, \quad \lambda_{33} \rightarrow \lambda_3, \quad \lambda_{12} \rightarrow \lambda_4, \quad \lambda_{31} \rightarrow \lambda_5, \quad (7)$$

$$\lambda_{23} \rightarrow \lambda_6, \quad \lambda'_{12} \rightarrow \lambda_7, \quad \lambda'_{31} \rightarrow \lambda_8, \quad \lambda'_{23} \rightarrow \lambda_9 \quad (8)$$

$$\lambda_1 \rightarrow \lambda''_{10}, \quad \lambda_3 \rightarrow \lambda''_{11}, \quad \lambda_2 \rightarrow \lambda''_{12}. \quad (9)$$

¹ We will only use the notation \mathbb{Z}'_2 in cases where the distinction becomes necessary.

B. Bounded from below and unitarity conditions

Any physically meaningful potential must be bounded from below (BFB). It is quite interesting that, although the $\mathbb{Z}_2 \times \mathbb{Z}_2$ 3HDM was first proposed by Weinberg in 1976 [40], there is still no known complete BFB necessary and sufficient conditions for this model. This is a testament to the intricacies involved in assessing the properties of a potential, including its vacua structure and BFB conditions.

When one has only one Higgs doublet, the possible vacua will unavoidably leave a remnant $U(1)$ gauge symmetry, corresponding to a massless photon. In contrast, when there are two or more Higgs doublets, the list of possible vacua always includes cases where there is a massless photon - the so-called neutral vacua - and cases where there is no remnant $U(1)$ gauge symmetry, corresponding to a massive “photon” - which are dubbed charge breaking (CB) vacua. By a conceptual extension, one classifies the “directions” in field space (now, not necessarily solutions of the stationarity equations) as neutral and CB, respectively. And, the BFB conditions along such directions are classified as BFB-n and BFB-c, respectively.

The necessary and sufficient conditions for the $\mathbb{Z}_2 \times \mathbb{Z}_2$ 3HDM potential to be BFB-n conditions were present in [41]. They find

$$\lambda_1 > 0, \lambda_2 > 0, \lambda_3 > 0, \quad (10)$$

$$\lambda_x > -2\sqrt{\lambda_1\lambda_2}, \lambda_y > -2\sqrt{\lambda_1\lambda_3}, \lambda_z > -2\sqrt{\lambda_2\lambda_3}, \quad (11)$$

$$\left\{ \lambda_x\sqrt{\lambda_3} + \lambda_y\sqrt{\lambda_2} + \lambda_z\sqrt{\lambda_1} \geq 0 \right\} \cup \left\{ \lambda_1\lambda_z^2 + \lambda_2\lambda_y^2 + \lambda_3\lambda_x^2 - 4\lambda_1\lambda_2\lambda_3 - \lambda_x\lambda_y\lambda_z < 0 \right\}, \quad (12)$$

where

$$\begin{aligned} \lambda_x &= \lambda_4 + \min(0, \lambda_7 - 2|\lambda''_{10}|), \\ \lambda_y &= \lambda_5 + \min(0, \lambda_8 - 2|\lambda''_{11}|), \\ \lambda_z &= \lambda_6 + \min(0, \lambda_9 - 2|\lambda''_{12}|). \end{aligned} \quad (13)$$

Later, Ref. [42] showed that the BFB-c conditions in [41] were sufficient but not necessary. Given the lack of necessary and sufficient conditions for BFB common to many 3HDM, Ref. [36] introduced a general method to obtain sufficient conditions for BFB-n and for BFB-c in any model. Here, we use the necessary and sufficient BFB-n conditions from [41] together with the sufficient BFB-c conditions from [36].

We use the perturbative unitarity conditions for the $\mathbb{Z}_2 \times \mathbb{Z}_2$ 3HDM found in [43] and in [44], which generalizes into complex coefficients and contains also the unitarity conditions for all other symmetry-constrained 3HDM.

III. THE POSSIBLE VACUA

This section is devoted to the identification of the possible vacua of the 3HDM $\mathbb{Z}_2 \times \mathbb{Z}_2$ model and the criteria ensuring that the inert vacuum corresponds to the global minimum. We start by describing the various vacua. Then, we explain how numerical and analytical explorations show that not all vacua are contained in Ref. [33].

A. Neutral vacua

The most general neutral vacuum configuration may be parametrized as

$$\langle \phi_1 \rangle = \begin{pmatrix} 0 \\ v_1 e^{i\xi_1} \end{pmatrix}, \quad \langle \phi_2 \rangle = \begin{pmatrix} 0 \\ v_2 e^{i\xi_2} \end{pmatrix}, \quad \langle \phi_3 \rangle = \begin{pmatrix} 0 \\ v_3 \end{pmatrix}. \quad (14)$$

Various of its distinct incarnations were studied in Ref. [33]. We follow their notation for the classification, which is shown in the upper part of Table I.

We want to get the conditions where the **2-Inert** minimum lies below all other neutral minima. Ref. [33] shows that DM1 and DM2 are always above **2-Inert**. As will be explained below, we found that guaranteeing that the **2-Inert** minimum lies below the other minima on the first part of Table I does *not* guarantee that it lies below our new minimum. This is easy to see with the following argument. The difference between the new FODMO' case and the FODMO case in Ref. [33] is that the former can be obtained from the latter with the substitution $\phi_2 \rightarrow i\phi_2$. As can be seen from Eqs. (3)-(4), this corresponds to $\lambda''_{10} \rightarrow -\lambda''_{10}$ and $\lambda''_{12} \rightarrow -\lambda''_{12}$.

Name	vevs	Symmetry of vacuum	Properties
Ews	$(0,0,0)$	$\mathbb{Z}_2 \times \mathbb{Z}'_2$	EW Symmetry
2-Inert	$(0, 0, v_3)$	$\mathbb{Z}_2 \times \mathbb{Z}'_2$	SM + 2 DM candidates
DM1	$(0, v_2, v_3)$	\mathbb{Z}_2	2HDM + 1 DM candidates
DM2	$(v_1, 0, v_3)$	\mathbb{Z}'_2	2HDM + 1 DM candidates
FODM1	$(0, v_2, 0)$	\mathbb{Z}_2	1 DM candidates + massless fermions
FODM2	$(v_1, 0, 0)$	\mathbb{Z}'_2	1 DM candidates + massless fermions
FODM0	$(v_1, v_2, 0)$	None	No DM candidate + massless fermions
N	(v_1, v_2, v_3)	None	3HDM no DM candidate
sCPv	$(v_1 e^{i\xi_1}, v_2 e^{i\xi_2}, v_3)$	None	Spontaneous CP violation
FODM0'	$(v_1, iv_2, 0)$	None	No DM candidate + massless fermions

TABLE I: Possible neutral vacua. The top of the table has all vacua found in Ref. [33]; the last line corresponds to a new vacuum. (See text for explanation.)

Now, in the FODM0 case, ensuring that **2-Inert** lies below involves $\lambda_7 + 2\lambda''_{10}$. But, since the vev $(v_1, iv_2, 0)$ is allowed, and since it is obtainable through $\lambda''_{10} \rightarrow -\lambda''_{10}$, we must also study $\lambda_7 - 2\lambda''_{10}$. This plausibility argument will be fully proved both analytically and numerically below.

B. Charge breaking vacua

In addition to normal vacua, where the photon is massless, there are also charge breaking (CB) vacua, and one must also guarantee stability against them. Those discussed in Ref. [33] can be found in the upper part of Table II.

Name	vevs		
CB1	$\begin{pmatrix} u_1 \\ c_1 \end{pmatrix}$	$\begin{pmatrix} u_2 \\ c_2 \end{pmatrix}$	$\begin{pmatrix} 0 \\ c_3 \end{pmatrix}$
CB2	$\begin{pmatrix} u_1 \\ 0 \end{pmatrix}$	$\begin{pmatrix} u_2 \\ c_2 \end{pmatrix}$	$\begin{pmatrix} 0 \\ c_3 \end{pmatrix}$
CB3	$\begin{pmatrix} u_1 \\ c_1 \end{pmatrix}$	$\begin{pmatrix} u_2 \\ 0 \end{pmatrix}$	$\begin{pmatrix} 0 \\ c_3 \end{pmatrix}$
CB4	$\begin{pmatrix} u_1 \\ c_1 \end{pmatrix}$	$\begin{pmatrix} u_2 \\ c_2 \end{pmatrix}$	$\begin{pmatrix} 0 \\ 0 \end{pmatrix}$
CB5	$\begin{pmatrix} 0 \\ c_1 \end{pmatrix}$	$\begin{pmatrix} u_2 \\ c_2 \end{pmatrix}$	$\begin{pmatrix} 0 \\ c_3 \end{pmatrix}$
CB6	$\begin{pmatrix} u_1 \\ c_1 \end{pmatrix}$	$\begin{pmatrix} 0 \\ c_2 \end{pmatrix}$	$\begin{pmatrix} 0 \\ c_3 \end{pmatrix}$
CB7	$\begin{pmatrix} u_1 \\ 0 \end{pmatrix}$	$\begin{pmatrix} u_2 \\ 0 \end{pmatrix}$	$\begin{pmatrix} 0 \\ c_3 \end{pmatrix}$
CB8	$\begin{pmatrix} u_1 \\ 0 \end{pmatrix}$	$\begin{pmatrix} 0 \\ 0 \end{pmatrix}$	$\begin{pmatrix} 0 \\ c_3 \end{pmatrix}$
CB9	$\begin{pmatrix} 0 \\ 0 \end{pmatrix}$	$\begin{pmatrix} u_2 \\ 0 \end{pmatrix}$	$\begin{pmatrix} 0 \\ c_3 \end{pmatrix}$
FOCB	$\begin{pmatrix} u_1 \\ c_1 \end{pmatrix}$	$\begin{pmatrix} u_2 \\ -\frac{u_1^* u_2}{c_1^*} \end{pmatrix}$	$\begin{pmatrix} 0 \\ 0 \end{pmatrix}$

TABLE II: Possible charge breaking (CB) vacua. The top of the table has all vacua found in Ref. [33]; the last line corresponds to a new vacuum. (See text for explanation.) In all cases, the vacua shown explicitly are assumed to be non-vanishing and unrelated; except on the last line, where the explicit relation $u_1^* u_2 + c_1^* c_2 = 0$ holds.

Ref. [33] studies the tadpole (stationarity) equations for CB vacua in their equations (3.34)-(3.38). Typically, those equations yield two solutions for the quartic parameters m_{11}^2 and/or m_{22}^2 . And, forcing their equality gives a constraint on the quartic couplings which, when used in the value of the potential at the minimum, imposes that the CB vacua CB1-CB9 always lie above the **2-Inert** vacuum [33].

As we will show below, we have found both analytically and numerically that there is, however, a further CB

vacuum, which we dub FOCB, corresponding to the last line of Table II. In hindsight, this arises because, under those very specific conditions ($c_3 = 0$ and $u_1^* u_2 + c_1^* c_2 = 0$), both m_{11}^2 and m_{22}^2 are unequivocally determined from the tadpole equations, with no further constraint on the quartic parameters. Again, the existence of this new and independent vacuum will be proved numerically and analytically below.

C. Numerical minimization

The most general vacuum to be compared with the 2-Inert minimum may be parametrized as [42]

$$\phi_1 = \sqrt{r_1} \begin{pmatrix} \sin \alpha_1 \\ \cos \alpha_1 \end{pmatrix} e^{i\beta_1}, \quad \phi_2 = \sqrt{r_2} e^{i\gamma} \begin{pmatrix} \sin \alpha_2 \\ \cos \alpha_2 \end{pmatrix} e^{i\beta_2}, \quad \phi_3 = \sqrt{r_3} \begin{pmatrix} 0 \\ 1 \end{pmatrix}. \quad (15)$$

The main result of Ref. [33] is that they only worry about the FODM1, FODM2 and FODM0 cases to make sure that the 2-Inert is the global minimum. They give conditions on the parameters of the potential, but for FODM0 it is simpler to make a numerical comparison of the value of the potential in the two situations.

To cross check their results we used the following method. We start by choosing some point in the (m_{ii}^2, λ_k) parameter space of Eqs. (3)-(4). We ensure that the point satisfies the BFB conditions explained in Section II B. Then, we impose

$$V_{2\text{Inert}} < V_X, \quad (16)$$

for all the X mentioned in Ref. [33]. Next we use the multi-step procedure explained in Ref. [45], utilizing CERN's Minuit library [46] in order to minimize the potential. In this method, we minimize the potential starting from a large number of random initial conditions for the parameters in Eq. (15). We found that out of 10000 points satisfying BFB and Eq. (16), there were still 161 (1.6%) that had a lower minima than $V_{2\text{Inert}}$. Note that this is not a numerical precision problem, because for those cases where $V_{2\text{Inert}}$ was indeed the global minimum we got precisely the value of the potential, and also $r_1 = r_2 = 0$ in the notation of Eq. (15). After adding the constraint

$$V_{2\text{Inert}} < V_{\text{FODM0}'}, \quad (17)$$

we still find points whose minimum lies below 2Inert. But, after adding the constraint

$$V_{2\text{Inert}} < V_{\text{FOCB}}, \quad (18)$$

our extensive minimization procedure no longer finds any global minimum below $V_{2\text{Inert}}$.

It turns out that all the new points correspond to $r_3 = 0$ and, thus, we study next that case analytically in detail.

IV. SOLVING THE MINIMIZATION EQUATIONS WHEN $r_3 = 0$

Here we perform an analytical study of the minimization, which agrees with the numerical results discussed previously.

A. The potential for $r_3 = 0$

For both new cases we have found numerically, FODM0' and FOCB, one has $r_3 = 0$. So, to have a better understanding of the situation, we consider the parameterization of Eq. (15) with $r_3 = 0$. Certainly, there are redundant angles, as we shall see in a moment. With these conditions the potential reads,

$$V = V_1 + \frac{1}{4} \lambda_7 r_1 r_2 f_7(\alpha_+, \alpha_-, \beta) + \frac{1}{2} \lambda_{10}'' r_1 r_2 f_{10}(\alpha_+, \alpha_-, \beta, \gamma), \quad (19)$$

where

$$V_1 = m_{11}^2 r_1 + m_{22}^2 r_2 + \lambda_1 r_1^2 + \lambda_2 r_2^2 + \lambda_4 r_1 r_2, \quad (20)$$

and we have defined

$$\alpha_+ = \alpha_1 + \alpha_2, \quad \alpha_- = \alpha_1 - \alpha_2, \quad \beta = \beta_1 - \beta_2, \quad (21)$$

already indicating that we need less angles to describe this situation, and where we also have defined,

$$\begin{aligned}
f_7(\alpha_+, \alpha_-, \beta) &= 2 - \cos(2\alpha_+)(-1 + \cos \beta) + \cos(2\alpha_-)(1 + \cos \beta), \\
f_{10}(\alpha_+, \alpha_-, \beta, \gamma) &= [\cos(2\alpha_+)(-1 + \cos \beta) + 2 \cos \beta + \cos(2\alpha_-)(1 + \cos \beta)] \cos(\beta - 2\gamma) \\
&\quad - 4 \cos(\alpha_-) \cos(\alpha_+) \sin \beta \sin(\beta - 2\gamma).
\end{aligned} \tag{22}$$

In Fig. 1, we plot f_7 versus f_{10} , for random values of α_+ , α_- , β , and γ . We see that $x = f_7 \in (0, 4)$, while

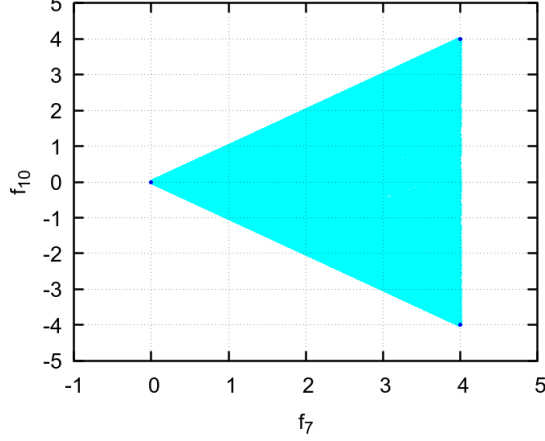


FIG. 1: Possible values of the functions f_7 and f_{10} required for the minimization of the angular part.

$y = f_{10} \in (-4, 4)$, lying between the lines $y = -x$ and $y = +x$. The angular part of our potential is of the form $g(x, y) = ax + by$, with $a = \lambda_7/4$ and $b = \lambda''_{10}/2$. It is easy to show that $g(x, y)$ cannot have extrema in the interior of the triangle in Fig. 1. And, assuming $\lambda_7 \neq \pm 2\lambda''_{10}$, it must have its extrema at the vertices of the triangle. The possibilities are, thus,

$$(f_7, f_{10}) = (0, 0) \implies g(0, 0) = 0, \tag{23}$$

$$(f_7, f_{10}) = (4, 4) \implies g(4, 4) = \lambda_7 + 2\lambda''_{10}, \tag{24}$$

$$(f_7, f_{10}) = (4, -4) \implies g(4, -4) = \lambda_7 - 2\lambda''_{10}. \tag{25}$$

The true minimum depends on which of Eqs. (23)-(25) lies the lowest. Notice that this is the only part that depends on λ_7 and/or λ''_{10} ; the candidates for extrema do *not* depend on λ_7 and/or λ''_{10} , for they can only lie at the vertices of the triangle regardless.

We conclude that

$$\lambda_7 > 2|\lambda''_{10}| \implies V_{\min} = V_1, \tag{26}$$

$$\lambda_7 < 2|\lambda''_{10}| \text{ and } \lambda''_{10} < 0 \implies V_{\min} = V_1 + r_1 r_2 (\lambda_7 + 2\lambda''_{10}), \tag{27}$$

$$\lambda_7 < 2|\lambda''_{10}| \text{ and } \lambda''_{10} > 0 \implies V_{\min} = V_1 + r_1 r_2 (\lambda_7 - 2\lambda''_{10}). \tag{28}$$

Equations (26)-(28) correspond, respectively, to the values obtained for the potential: i) in our new charge breaking case FOCB; ii) in the case FODMO of Ref. [33]; and iii) in our new case FODMO'.

By looking at the extrema conditions for f_7 and f_{10} in Appendix B, one can show that (26) occurs for one of the following angle combinations:

$$i) \quad \beta = 0 \text{ and } \cos \alpha_- = 0, \tag{29}$$

$$ii) \quad \beta = \pi \text{ and } \cos \alpha_+ = 0, \tag{30}$$

$$iii) \quad \sin \beta \neq 0 \text{ and } \cos(2\alpha_+) = \cos(2\alpha_-) = -1. \tag{31}$$

Similarly, by looking at the extrema conditions for f_7 and f_{10} , one can show that (27) and (28) occur, respectively, for one of the following angle combinations:

$$i) \quad \beta = 0 \text{ and } \sin \alpha_- = 0 \text{ and } \cos(2\gamma) = \pm 1, \tag{32}$$

$$ii) \quad \beta = \pi \text{ and } \sin \alpha_+ = 0 \text{ and } \cos(2\gamma) = \pm 1, \tag{33}$$

$$iii) \quad \sin \beta \neq 0 \text{ and } (\alpha_+, \alpha_-) = (0, 0), (\pi, \pi) \text{ and } \cos(2\beta - 2\gamma) = \pm 1, \tag{34}$$

$$iv) \quad \sin \beta \neq 0 \text{ and } (\alpha_+, \alpha_-) = (0, \pi), (\pi, 0) \text{ and } \cos(2\gamma) = \pm 1. \tag{35}$$

We have crossed checked our results with our numerical method of finding the global minimum and they completely agree.

V. SETTING UP THE SCAN

In the previous sections we discussed in detail how to ensure that our **2-Inert** is indeed the global minimum. We used implicitly the relations found for this minimum. Namely, we take $v_1 = v_2 = 0$, $v_3 = v$ and find

$$m_h^2 = 2\lambda_3 v^2, \quad v^2 = -\frac{m_{33}^2}{\lambda_3}, \quad (36)$$

requiring $\lambda_3 > 0$ (already needed for BFB) and $m_{33}^2 < 0$. The fields can be parametrized as

$$\phi_1 = \left(\frac{H_1^+}{\sqrt{2}} (H_1 + iA_1) \right), \quad \phi_2 = \left(\frac{H_2^+}{\sqrt{2}} (H_2 + iA_2) \right), \quad \phi_3 = \left(\frac{G^+}{\sqrt{2}} (v + h + iG_0) \right). \quad (37)$$

Since the vacuum does not break the $\mathbb{Z}_2 \times \mathbb{Z}_2$ symmetry in Eq. (1), all states are unmixed; they are already in the mass basis. Moreover, G^0 and G^+ are the would-be Goldstone bosons, which, in the unitary gauge, become the longitudinal components of the Z^0 and W^+ gauge bosons, respectively.

It proves useful² to define [33]

$$\Lambda_1 = \frac{1}{2} (\lambda_4 + \lambda_7 + 2\lambda_{10}''), \quad \bar{\Lambda}_1 = \frac{1}{2} (\lambda_4 + \lambda_7 - 2\lambda_{10}''), \quad (38)$$

$$\Lambda_2 = \frac{1}{2} (\lambda_6 + \lambda_9 + 2\lambda_{12}''), \quad \bar{\Lambda}_2 = \frac{1}{2} (\lambda_6 + \lambda_9 - 2\lambda_{12}''), \quad (39)$$

$$\Lambda_3 = \frac{1}{2} (\lambda_5 + \lambda_8 + 2\lambda_{11}''), \quad \bar{\Lambda}_3 = \frac{1}{2} (\lambda_5 + \lambda_8 - 2\lambda_{11}''). \quad (40)$$

The other masses are given by

$$m_{H_1}^2 = m_{11}^2 + \frac{1}{2} (\lambda_5 + \lambda_8 + 2\lambda_{11}'') v^2 \equiv m_{11}^2 + \Lambda_3 v^2, \quad (41)$$

$$m_{A_1}^2 = m_{11}^2 + \frac{1}{2} (\lambda_5 + \lambda_8 - 2\lambda_{11}'') v^2 \equiv m_{11}^2 + \bar{\Lambda}_3 v^2, \quad (42)$$

$$m_{H_1^\pm}^2 = m_{11}^2 + \frac{1}{2} \lambda_5 v^2, \quad (43)$$

$$m_{H_2}^2 = m_{22}^2 + \frac{1}{2} (\lambda_6 + \lambda_9 + 2\lambda_{12}'') v^2 \equiv m_{22}^2 + \Lambda_2 v^2, \quad (44)$$

$$m_{A_2}^2 = m_{22}^2 + \frac{1}{2} (\lambda_6 + \lambda_9 - 2\lambda_{12}'') v^2 \equiv m_{22}^2 + \bar{\Lambda}_2 v^2, \quad (45)$$

$$m_{H_2^\pm}^2 = m_{22}^2 + \frac{1}{2} \lambda_6 v^2. \quad (46)$$

The conditions for a local minimum are

$$v^2 = -\frac{m_{33}^2}{\lambda_3} > 0, \quad \Lambda_2 > -m_{22}^2/v^2, \quad \Lambda_3 > -m_{11}^2/v^2, \quad (47)$$

but, if we take the masses as input parameters, these will be automatically satisfied. The value of the potential at the minimum is

$$V_{2\text{Inert}} = -\frac{m_{33}^4}{4\lambda_3}. \quad (48)$$

As mentioned, we ensure that $V_{2\text{Inert}}$ lies below the value of the potential at the other local extrema, whose explicit expressions can be found in Appendix A.

² Our definition of Λ_1 agrees with the vertex in Fig. 9b of [33], but not with their Eqs. (2.39), (5.7)-(5.8).

We take

$$v = 246 \text{ GeV}, \quad m_h = 125 \text{ GeV}, \quad (49)$$

as fixed inputs. We follow Ref. [33] and choose as our free parameters

$$m_{H_1}^2, m_{H_2}^2, m_{A_1}^2, m_{A_2}^2, m_{H_1^\pm}^2, m_{H_2^\pm}^2, \Lambda_1, \Lambda_2, \Lambda_3, \lambda_1, \lambda_2, \lambda_4, \lambda_7. \quad (50)$$

All other parameters of the scalar potential can be extracted from Eq. (36)-(46). We choose random values for the remaining parameters in the set of Eq. (50), in the ranges

$$\begin{aligned} \Lambda_1, \Lambda_2, \Lambda_3, \lambda_1, \lambda_2, \lambda_4, \lambda_7 &\in \pm [10^{-3}, 10]; \\ m_{H_1}, m_{H_2}, m_{A_1}, m_{A_2} &\in [50, 1000] \text{ GeV}; \\ m_{H_1^\pm}, m_{H_2^\pm} &\in [70, 1000] \text{ GeV}, \end{aligned} \quad (51)$$

with the chosen condition that $m_{H_1} < m_{H_2}$, without loss of generality. The lower limit on the mass of the charged scalars comes from Ref. [47]. Although this bound has not been established within the context of the current model of two component DM, we take it as a conservative lower bound on the masses of all charged scalars.

For the interactions with fermions and gauge bosons, it is assumed that all such SM fields transform into themselves under $\mathbb{Z}_2 \times \mathbb{Z}_2$. Thus, Eq. (1) implies that *all* fermion fields only couple with ϕ_3 . This is a so-called Type-I model. Since the Yukawa couplings are identical to the SM ones, there are no FCNCs at tree-level. Moreover, as the charged scalars are inert and lack coupling to fermions, they bypass many of the constraints found in the usual 2HDMs. Notably, flavour bounds on the charged scalar masses, such as from $B \rightarrow X_s \gamma$ are trivially satisfied. As the fields in Eq. (37) are already in the mass basis, there are thus three sectors: the dark- \mathbb{Z}_2 sector, constituted by the fields in ϕ_1 ; the dark- \mathbb{Z}'_2 sector, constituted by the fields in ϕ_2 ; and the active or SM sector, constituted by the fields in ϕ_3 and all SM fermions. Connections among different sectors can only occur due to gauge bosons or due to the cubic and quartic interactions of the Higgs potential.

We have generated `FeynMaster` [48, 49], and, through it, `FeynRules` [50] model files which yield all Feynman rules³ and were used to generate an input file for `micrOMEGAs 6.0.5` [51].

Our numerical scan proceeds in the following fashion. We start by taking a random value for the parameters (50) within the intervals (51). The values of $\Lambda_1, \Lambda_2, \Lambda_3, \lambda_1, \lambda_2, \lambda_4$, and λ_7 were scanned log-uniformly; all other input parameters were scanned uniformly. For the constraints in this section, all parameters were actually scanned over. For the plots in section VIII, extensive dedicated scans around points yielding the correct relic density were performed. In some DM mass regions, points were easier to generate; in other regions, a good point was very hard to come by. We continued this process until a reasonable density in each plot was obtained. As mentioned above, we apply the constraints from BFB and global minimum. Then, as a sanity check, we confirm numerically that indeed no lower-lying minimum is found. Next, we impose perturbative unitarity [43, 44], and compliance with the experimental oblique radiative parameter STU [52], utilizing the general formulae in [53]. We calculate all processes at lowest non-trivial order and take all input parameters at the electroweak scale.

VI. FURTHER EXPERIMENTAL CONSTRAINTS

A. Collider constraints

We have adapted our in-house scanning program including already the latest LHC bounds on the h_{125} signal strengths with the full Run 2 data collected at 13 TeV, for the different production and decay modes, following the ATLAS results⁴ summarized in Fig. 3 of [54]. For comparison with these collider experiments, we consider only the decay contributions of the lowest non-vanishing order in perturbation theory when comparing with the coupling

³ The complete and consistent set of all Feynman Rules for this model may be found at the url <https://porthos.tecnico.ulisboa.pt/~romao/Work/arXiv/3HDMZ2xZ2-Inert2/>.

⁴ The generic agreement between ATLAS and CMS measurements implies that our conclusions will not be altered significantly if we use instead CMS results or a suitable combination and ATLAS and CMS results.

modifiers of the most recent ATLAS fit result Ref. [54], within 2σ . For a specific production mechanism and decay channel, the Higgs signal strength is defined as:

$$\mu_i^f = \left(\frac{\sigma_i^{\text{3HDM}}(pp \rightarrow h)}{\sigma_i^{\text{SM}}(pp \rightarrow h)} \right) \left(\frac{\text{BR}^{\text{3HDM}}(h \rightarrow f)}{\text{BR}^{\text{SM}}(h \rightarrow f)} \right), \quad (52)$$

with the subscript ‘ i ’ corresponding to the production mode and the superscript ‘ f ’ to the decay channel of the 125 GeV Higgs scalar. The relevant production mechanisms considered are gluon fusion (ggF), vector boson fusion (VBF), associated production with a vector boson (VH , $V = W$ or Z), and associated production with a pair of top quarks (ttH). The SM cross section for the gluon fusion process is calculated using HIGLU [55], and for the other production mechanisms we use the prescription of Ref. [56]. The final states in the decay channels considered are $f = WW, ZZ, b\bar{b}, \gamma\gamma$ and $\tau^+\tau^-$. The upper limit on the Higgs total decay width is set by Ref. [57] at:

$$\Gamma_{\text{tot}} \leq 9.1 \text{ MeV}. \quad (53)$$

We forbid decays of SM gauge bosons into the new scalars by enforcing:

$$m_{H_i} + m_{H_i^\pm} \geq m_W^\pm, \quad m_{A_i} + m_{H_i^\pm} \geq m_W^\pm, \quad m_{H_i} + m_{A_i} \geq m_Z, \quad 2m_{H_i^\pm} \geq m_Z. \quad (54)$$

Taking into account the LEP 2 results re-interpreted for the I(1+1)HDM, we exclude the region of masses where the following conditions are simultaneously satisfied [58] ($i = 1, 2$):

$$m_{A_i} \leq 100 \text{ GeV}, \quad m_{H_i} \leq 80 \text{ GeV}, \quad |m_{A_i} - m_{H_i}| \geq 8 \text{ GeV}. \quad (55)$$

In order to evade the bounds from long-lived charged particle searches given in Ref. [59], we set the upper limit on the charged scalar lifetime of $\tau \leq 10^{-7} \text{ s}$.

The surviving points were then passed through HiggsTools 1.1.3 [60], imposing current bounds from searches for additional scalars.

B. DM constraints

Our results for the relic density, scattering amplitudes and annihilation cross section are obtained using the implementation of this model in micrOMEGAs 6.0.5 [51], which we have constructed.

We calculate the dark matter relic density as the sum of the contributions of each DM candidate:

$$\Omega_T h^2 = \Omega_1 h^2 + \Omega_2 h^2, \quad (56)$$

and apply the limits obtained by the Planck experiment [61]⁵:

$$\Omega_T h^2 = 0.1200 \pm 0.0012. \quad (57)$$

The strongest direct detection limit from dark matter-nucleon scattering is currently provided by Ref. [64]. To compare directly with the experimental limit, we follow the method presented in [65] of computing the normalized cross section of DM on a point-like nucleus (taken to be xenon)

$$\sigma_{\text{SI}}^{\text{Xe},k} = \frac{4\mu_k^2}{\pi} \frac{(Zf_p + (A-Z)f_n)^2}{A^2}, \quad (58)$$

with μ_k the reduced mass of the DM candidate and f_p, f_n the amplitudes for protons and neutrons. As there are two dark matter candidates, we rescale the obtained cross section for each DM candidate by the relative density of the component:

$$\sigma_{\text{SI}}^{r,k} = \sigma_{\text{SI}}^{\text{Xe},k} \xi_k, \quad (59)$$

⁵ Alternatively, one could adopt a more permissive range. Indeed, some models have been studied where loop effects can induce corrections to the relic density which are of the order of 10% [62, 63]; this lead the authors of [29] to consider instead the augmented range $0.094 < \Omega_T h^2 < 0.142$. We will keep to the Planck constraint in (57).

where

$$\xi_k = \frac{\Omega_k}{\Omega_T}. \quad (60)$$

To deal with indirect detection constraints, we follow closely the strategy adopted in [29]. We start by using our `micrOMEGAs 6.0.5` model implementation in order to calculate the thermally averaged cross section for DM annihilation (or co-annihilation, or DM conversion) times velocity $\langle\sigma v\rangle$. Current Fermi-LAT limits for indirect DM detection through photons [66] range from $\langle\sigma v\rangle \approx 3 \times 10^{-26} \text{cm}^3/\text{s}$, for light DM, to around $\langle\sigma v\rangle \approx 10^{-25} \text{cm}^3/\text{s}$, for heavier DM. As in [29], we find that the $\langle\sigma v\rangle$ which are in reach of Fermi-LAT arise mainly from annihilation decays into VV . So we sum only the WW and ZZ final states, assuming a similar spectrum, which we dub $\langle\sigma v\rangle_{VV}$, and we limit it to the 95% CL bound from Fermi-LAT [66].

Searches for anti-protons with AMS-02 [67, 68] yield the most stringent constraints for WIMP DM. Again, we consider $\langle\sigma v\rangle_{VV}$ and use the bounds obtained in [69]. We also comment briefly on limits from H.E.S.S. [70], a Cherenkov gamma ray, ground-based telescope, which points to the central region of the Milky Way. This yields the strongest ID constraints for DM masses from $\sim 500 \text{GeV}$ upwards.

VII. SOME INTERESTING PROCESSES

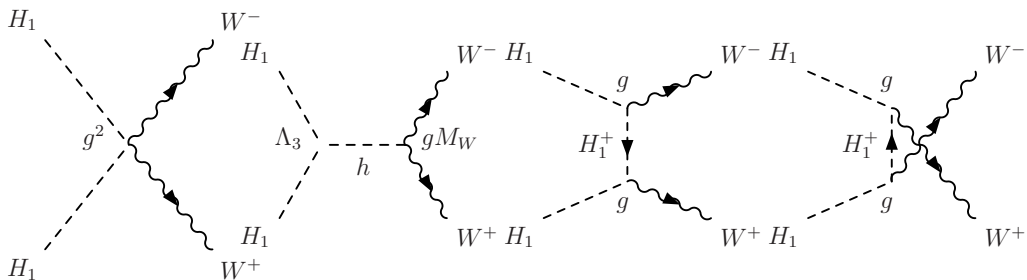


FIG. 2: Feynman diagrams for $H_1H_1 \rightarrow WW$.

Before we proceed, it is interesting to describe some of the classes of processes achievable in this very rich model. Indeed, we have:

- (vanilla) annihilation: e.g. $H_1H_1 \rightarrow b\bar{b}$,
- co-annihilation: e.g. $A_1H_1 \rightarrow b\bar{b}$,
- co-scattering: e.g. $H_1^+W^- \rightarrow A_1Z$,
- DM conversion: e.g. $H_2H_2 \rightarrow H_1H_1$.

There are, however, no semi-annihilations processes $x_i x_j \rightarrow x_k \text{SM}$, such as appears in [27]. Fig. 2 shows the Feynman diagrams for $H_1H_1 \rightarrow WW$. The Feynman diagrams for $H_1H_1 \rightarrow ZZ$ are obtained from Fig. 2 with the substitutions $W^\pm \rightarrow Z$, $H_1^\pm \rightarrow A_1$.

This model has DM conversion processes between the DM sector 1 and the DM sector 2:

- $H_2H_2 \rightarrow H_1H_1$: quartic ($\sim \Lambda_1$), and through h ($\sim \Lambda_2\Lambda_3$);
- $H_2H_2 \rightarrow A_1A_1$: quartic ($\sim \bar{\Lambda}_1$), and through h ($\sim \Lambda_2\bar{\Lambda}_3$);
- $H_2A_2 \rightarrow H_1A_1$: quartic ($\sim \lambda''_{10}$), and through Z ($\sim g^2$).

We show the Feynman diagrams for these DM conversion processes in Figs. 3, 4, and 5.

The numerical results to be discussed below include all processes, which arise out of our implementation of the model in `micrOMEGAs 6.0.5`. The authors of Ref. [33] choose to concentrate on the mass region $m_h/2 < m_{H_1} < 80 \text{GeV}$ and $m_{H_2} \simeq 100 \text{GeV}$. We extend significantly the analysis by considering all available parameter space. Not surprisingly, we find different conclusions. In particular, we find many situations in which both DM components can contribute equally to the relic density. We also find wide regions of parameter space where the possibility that the lighter DM component is mainly probed through direct nuclear recoil while the heavier DM component is probed in indirect DM detection does not hold. This will be discussed next.

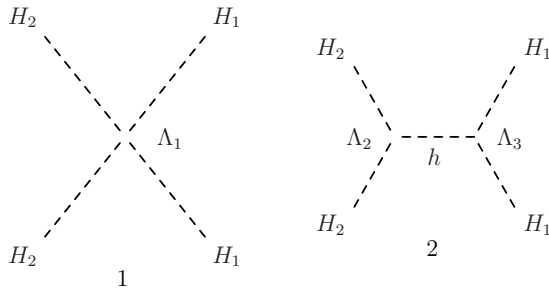


FIG. 3: Feynman diagrams for the DM conversion processes $H_2H_2 \rightarrow H_1H_1$.

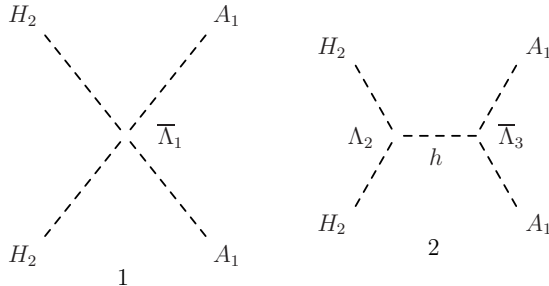


FIG. 4: Feynman diagrams for the DM conversion processes $H_2H_2 \rightarrow A_1A_1$.

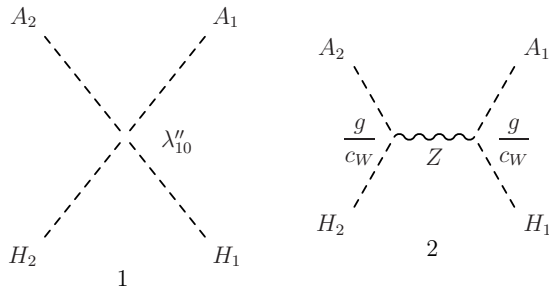


FIG. 5: Feynman diagrams for the DM conversion processes $H_2A_2 \rightarrow H_1A_1$.

VIII. RESULTS AND DISCUSSION

In the IDM, the DM mass is constrained to two regions. The reason is the following. The annihilation of the DM particle into WW (equivalent to that in Fig. 2) is controlled by a gauge coupling and, thus, it is not tunable. For the most part, it leads to a decay rate so high that it depletes the IDM DM candidate, making its relic density under-abundant. This is avoided for $m_{\text{dm}} \gtrsim 500\text{GeV}$ if all “dark” scalars (H , A , and H^\pm) have similar masses. Below the W threshold, the annihilation proceeds mostly into $b\bar{b}$; this depends on the DM-Higgs coupling, which is tunable to comply with the relic density. However, that requires large couplings, which are precluded by direct detection. The exception occurs around $m_{\text{dm}} \simeq m_h/2$ where the annihilation has a resonance, allowing for a fit to the relic density with a coupling low enough to comply with direct detection constraints.

The situation is both similar and different in our two component DM $\mathbb{Z}_2 \times \mathbb{Z}_2$ 3HDM. This is best seen with the help of Fig. 6, where we show the values of $\langle\sigma v\rangle$ for H_1 (H_2) annihilation into $b\bar{b}$ and VV as a function of m_{H_1} . First, we note that above the W threshold $\langle\sigma v\rangle_{VV} \gg \langle\sigma v\rangle_{b\bar{b}}$ for both H_1 and H_2 . Second, for H_1 , $\langle\sigma v\rangle_{b\bar{b}}$ can be very large for low values of m_{H_1} , as in the IDM. Thus, if H_1 were the only DM component, combining relic density and direct detection constraints would lead to the same mass regions as in the IDM. However, we can force m_{H_1} into the intermediate mass range, by requiring that it is H_2 which is mostly responsible for the relic density. This can be seen in Fig. 7. Notice also that for small m_{H_1} there are two possibilities. For any value of m_{H_2} , one can have H_1 be the major relic density component. On the other hand, for $500\text{GeV} \lesssim m_{H_2} \lesssim 600\text{GeV}$, one can have H_2 be the major relic density component. Moreover, one can find quite a number of interesting points where $\Omega_1 \simeq \Omega_2$. These occur for the H_1 mass regions which would be allowed in the IDM. The reason is simple; H_1 would be able to allow for all

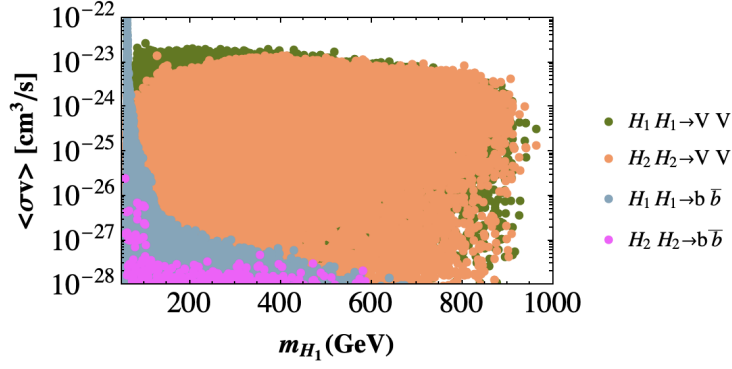


FIG. 6: $\langle\sigma v\rangle$ for H_1 (H_2) annihilation into $b\bar{b}$ and VV as a function of m_{H_1} . The colour codes are in the figure.

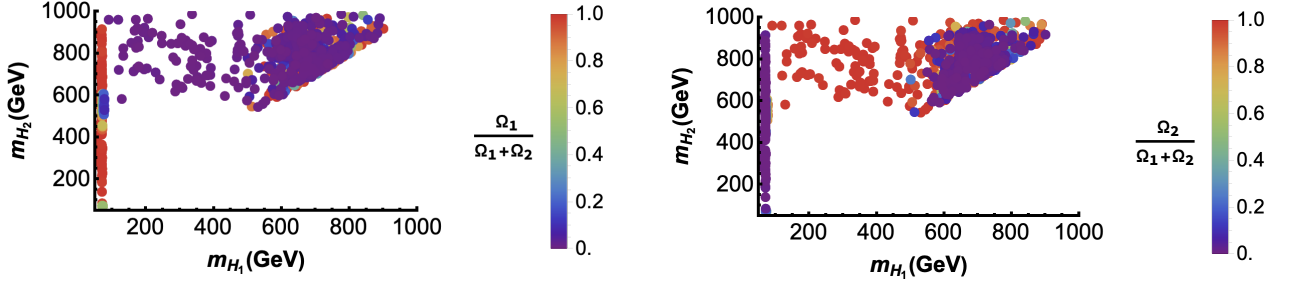


FIG. 7: Range of allowed (m_{H_1}, m_{H_2}) masses with a “temperature” colour code for Ω_1/Ω_T (Ω_2/Ω_T) on the left (right). Both plots have the same information but were included to aid the eye. These points have passed all theory, collider and astrophysical constraints.

the relic density, and one can tune it down for 50%, while tuning the H_2 parameters to account for the remainder 50%. Finally, we note that if a DM component has a mass between $\sim 100\text{GeV}$ and $\sim 500\text{GeV}$, then it is guaranteed to give a very suppressed contribution to the total relic density.

There is one relevant issue concerning Fig. 6. One might worry that there are significant contributions from $\langle\sigma v\rangle_{hh}$. We have checked that this is the case if we do not impose that Ω_T must equal the measured relic density. However, once we impose the Planck limit in Eq. (57), the dominant contributions are those shown in Fig. 6. Albeit in a different model, this is also what was found in Ref. [29]. This will be important to the discussion on indirect detection below.

But first, we turn to the constraints from direct detection shown in Fig. 8. The lines shown have the following

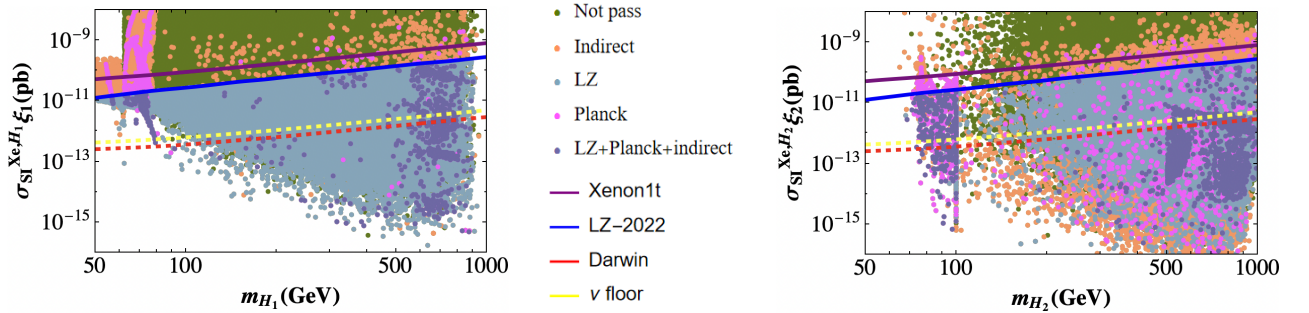


FIG. 8: Direct detection constraints on H_1 (H_2) on the left (right) figure. See text for details.

origins: i) the solid purple line refers to the XENON1T [71], which is included as recast limits inside `micrOMEGAS` 6.0.5; ii) the solid blue line refers to the current LUX-ZEPLIN (LZ) bound [64]; iii) the dashed red line corresponds to the expected reach of the DARWIN experiment [72]; iv) the dashed yellow line corresponds to the neutrino floor, as presented in [73]. As for the points shown, all have passed theory and collider constraints. The colour code refers to the additional astrophysical constraints as follows: i) the green points have passed theory and collider constraints,

but failed all of the relic density, direct and indirect limits; ii) the orange points have agreement with Fermi-LAT's indirect detection bounds [66], but fail both Planck and LZ; iii) the gray points Pass LZ, but fail Planck (some pass Fermi-LAT; some do not); iv) the pink points achieve the correct relic density, but failed either LZ or Fermi-LAT; finally, v) the dark-purple points pass all current astrophysical constraints.

Let us concentrate first on Fig. 8-left. The presence of red and orange points above the LZ line shows that, in agreement with our previous discussion, this constraint from direct detection is relevant for low H_1 masses. Remarkably, for such low masses the DARWIN experiment will be able to exclude many points. In contrast, many points with high H_1 masses will not be invalidated by DARWIN. And, since this exclusion is expected to lie below the neutrino floor, other collider and/or astrophysical probes must be used. Turning to Fig. 8-right, we see that direct detection may also constrain H_2 . This is more clearly seen in a plot as a function of m_{H_1} , as in Fig. 9. However, looking at

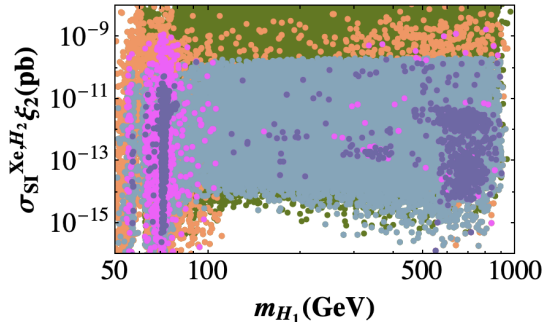


FIG. 9: Constraints on $\sigma_{\text{SI}}^{\text{Xe},H_2} \xi_2$ as a function of m_{H_1} . The colours of points have the same meaning as in Fig. 8. Notice that the curves for experimental constraints are not appropriate for this graph.

the pink and dark-purple points in Fig. 9 for low values of m_{H_1} it is possible that direct detection probes H_1 , while it does not affect H_2 , in accordance with the special case discussed in [33].

Note that the appearance of green points bellow all exclusion lines in one of the plots in Fig. 8 is due to the fact that, although the point passes the direct detection for the corresponding DM component, it does not pass it for the other DM component.

We now turn to the constraints arising from indirect detection. As mentioned, our strategy was to prove that $\langle\sigma v\rangle_{VV}$ dominates for most of the parameter space, use the lines determined by the authors of Ref. [69] together with gamma ray searches for dark matter [66, 70]. The exception occurs for small masses, where we apply the $\langle\sigma v\rangle_{bb}$ lines also obtained by the authors of Ref. [69] and Fermi-LAT experiment [66].

Fig. 10-left shows the total $\langle\sigma v\rangle$. The plots have 200000 points (in fact, we generated 1 million points, but the

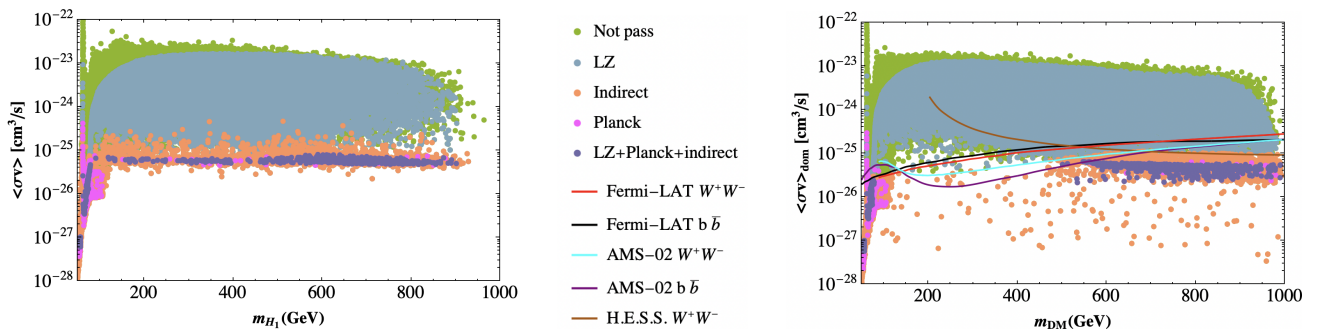


FIG. 10: The colours of the points have the same meaning as in Fig. 8. The left figure shows the total $\langle\sigma v\rangle$ as a function of m_{H_1} . The right figure shows the dominant contribution to $\langle\sigma v\rangle$ as a function of the mass of the DM candidate, m_{DM} , which corresponds to the $\langle\sigma v\rangle$ plotted on the vertical axis. The lines coming from Fermi-LAT [66] and H.E.S.S. [70] assume a Navarro-Frenk-White (NFW) DM density profile and the AMS-02 [67] lines correspond to the conservative approach derived in Ref. [69], with the colour codes also shown in the figure.

conclusions are not altered). The colours of the points have the same meaning as in Fig. 8. The red points have passed Planck bounds but may, or not, have passed the bounds from indirect detection. However, we found that, out of 2761 points that pass Planck, only 36 are ruled out by indirect detection, and that this occurs only for masses of H_1 between $\sim 62\text{GeV}$ and $\sim 66\text{GeV}$, where the dominant contribution is $\langle\sigma v\rangle_{bb}$. This is also seen on Fig. 10-right, where

we plot the dominant contribution to $\langle\sigma v\rangle$ as a function of the mass of the DM candidate, m_{DM} , which corresponds to the (dominant) $\langle\sigma v\rangle$ plotted on the vertical axis. This is to be compared with the exclusion lines for $\langle\sigma v\rangle_{VV}$ and $\langle\sigma v\rangle_{bb}$ corresponding to H_1 or H_2 ; whichever yields the dominant $\langle\sigma v\rangle$. The lines come from Ref. [69] and refer to exclusions extrapolated from Fermi-LAT [66] (in red for VV and in black for bb), and from AMS-02 [67] (in light-blue for VV and in purple for bb). We also include (in a solid brown line) a limit coming from H.E.S.S. [70], which is important for DM masses above ~ 500 GeV. As a result, we can conclude that, except for those very specific 36 points, the Planck constraints (almost) guarantee that the indirect detection will be ineffectual. Again, the black points pass every constraint.

We now turn to the interplay between direct and indirect detection. Fig. 11-left (-right) contains points for which the dominant direct detection cross-section is due to H_1 (H_2). In both, we plot $\langle\sigma v\rangle_{VV}$ for H_1 over the sum of $\langle\sigma v\rangle_{VV}$ for H_1 and H_2 . Concentrating on Fig. 11-left, we learn that, whilst direct detection is dominated by H_1 , H_1 can,

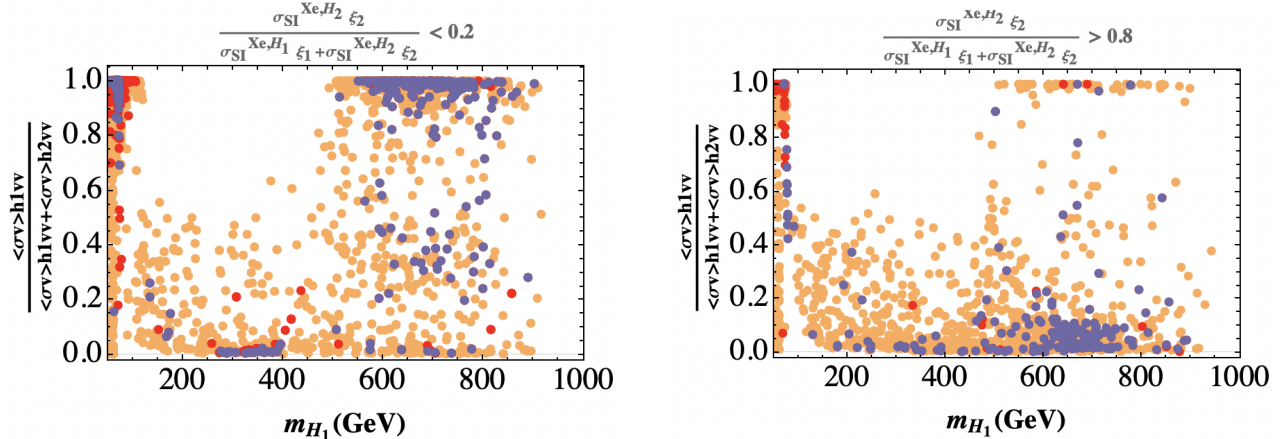


FIG. 11: The orange points pass the indirect detection bounds; the red ones achieve the correct density; and the dark-purple points pass all astrophysical constraints. On the left (right) we show points where direct detection is dominated by H_1 (H_2).

in some cases, give the dominant contribution to indirect detection, while, in other cases, it is H_2 which gives the dominant contribution to indirect detection. Conversely, on Fig. 11-right, we learn that, whilst direct detection is dominated by H_2 , H_1 can, in some cases, give the dominant contribution to indirect detection, while, in other cases, it is H_2 which gives the dominant contribution to indirect detection. That is, depending on the parameters of the model, including m_{H_1} , we can have all four possible combinations.

Notice the following feature on both plots in Fig. 11. When m_{H_1} lies roughly between 100 GeV and 500 GeV, it can never be the dominant contribution to indirect detection signals. This is also the region where H_1 cannot be the dominant contribution to the relic density. This is the previously referred relation between relic density and indirect detection.

Recall, that since we have only one active scalar, all tree level 125 GeV Higgs couplings are as in the SM model. It is only in loop mediated (or loop corrections to tree level) decays that we are sensitive to the dark sectors. As an example, we show results for the $h \rightarrow \gamma\gamma$ decay in Fig. 12. We start by noticing that, after theoretical and LHC

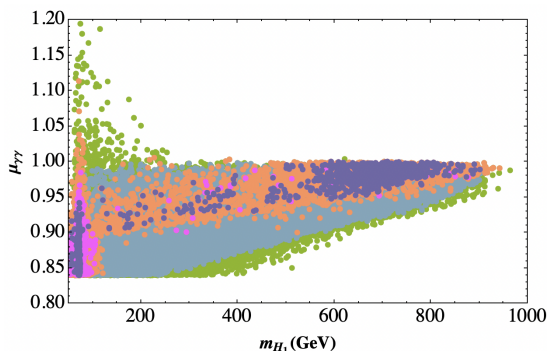


FIG. 12: Constraints on $\mu_{\gamma\gamma}$ as a function of m_{H_1} . The colours of points have the same meaning as in Fig. 8.

constraints, there is a region where $\mu_{\gamma\gamma}$ could exceed unity. Although not completely apparent from the figure, this region only starts after $M_{H_1} > m_h/2$, and decreases sharply until around $m_{H_1} \sim 300\text{GeV}$. This is exactly the same that one finds in the IDM; compare, for example, with figure 3-left of [74]; see also [75]. However, this region is already excluded by the LZ direct detection bound. Thus, in the $\mathbb{Z}_2 \times \mathbb{Z}_2$ 3HDM, current astrophysical bounds force $\mu_{\gamma\gamma} \lesssim 1$.

As for $h \rightarrow Z\gamma$, the current measurement of $\mu_{Z\gamma} = 2.2 \pm 0.7$ [76–78], still has large errors. Nonetheless, if its central value remained with shrinking errors, it would constitute a definite sign of new Physics. We show the results for the $\mu_{\gamma\gamma}$ versus $\mu_{Z\gamma}$ within the $\mathbb{Z}_2 \times \mathbb{Z}_2$ 3HDM in Fig. 13. One sees a very strong correlation between $\mu_{\gamma\gamma}$ and $\mu_{Z\gamma}$, due to

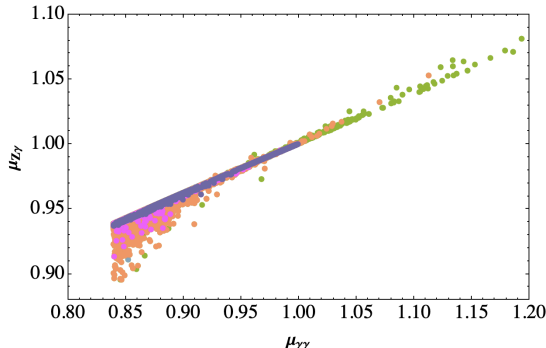


FIG. 13: Constraints on the $\mu_{\gamma\gamma} - \mu_{Z\gamma}$ plane. The colours of points have the same meaning as in Fig. 8.

the fact that very similar new virtual charge Higgs diagrams are involved in both cases.⁶ As a result, should a more precise measurement of $\mu_{Z\gamma}$ uncover new physics, the $\mathbb{Z}_2 \times \mathbb{Z}_2$ 3HDM would be ruled out together with the SM.

IX. CONCLUSION

Recently there has been renewed interest in multi-component DM models. We focus our attention on a $\mathbb{Z}_2 \times \mathbb{Z}_2$ symmetric 3HDM with a double inert vacuum. We start by reassessing the possible solutions of the stationarity equations, making sure that ours is the absolute minimum. We found new relevant minima, which we dub FODM0' and FOCB. To be certain that we keep all the points that are global minima, we have to compare not only with the FODM1, FODM2 and FODM0, but also with the new cases, FODM0' (Eq. (A30) and FOCB (Eq. (A47)). We obtained explicit expressions for all the cases and therefore it is easy to compare. We also include unitarity, BFB and conformance with the oblique parameters S , T , and U .

After this step, we subject the parameter space of our model to all current collider constraints, including limits in the 125GeV couplings, searches for extra scalars and flavour observables. We then concentrate on the implications from relic density, DD and ID of DM. By performing a wide scan, we found that simple implications obtained when concentrating on small regions of parameter space cease to be valid, and a much richer pallet of possibilities emerges. In particular, we found regions where one can have two DM candidates contributing equally to the relic density. The whole mass range for a given component can be populated in the $\mathbb{Z}_2 \times \mathbb{Z}_2$ model, even for intermediate mass regions that require the other component to dominate the relic density calculation. We include the future sensitivity of DD experiments that are expected to reach the high mass section of the neutrino fog without being able to invalidate the model, thus requiring complementary probes.

We hope that this work will entice the community to look closer at this stimulating model. In particular, it will be interesting to explore its implication to more detailed collider observables, such as monojets with large missing transverse energy, mono- Z or multi-lepton signals. In addition, one may also seek exploratory predictions for the reach of proposed future colliders. We leave this for a future publication.

⁶ It is viable to uncorrelate $\mu_{Z\gamma}$ from $\mu_{\gamma\gamma}$ in multi-Higgs models where the Z couples to two different charged Higgses [79].

Acknowledgments

This work is supported in part by the Portuguese Fundação para a Ciência e Tecnologia (FCT) under Contracts CERN/FIS-PAR/0002/2021, UIDB/00777/2020, and UIDP/00777/2020; these projects are partially funded through POCTI (FEDER), COMPETE, QREN, and the EU. The work of R. Boto is also supported by FCT with the PhD grant PRT/BD/152268/2021.

Appendix A: Mass formulas and conditions for local minima

In this Appendix we present the formulas for the scalar masses under the various minima of interest. Requiring that the mass squared are positive is akin to guaranteeing that the corresponding extreme is indeed a local minimum.

1. 2-Inert

This case can be found in Eq. (36)-(48) of Section V.

2. FODM1

In this case we have $v_1 = 0, v_2 \neq 0, v_3 = 0$. The minimization gives

$$v_2^2 = -\frac{m_{22}^2}{\lambda_2}, \quad (\text{A1})$$

implying $m_{22}^2 < 0$ as $\lambda_2 > 0$ from BFB. For the masses we have

$$m_{H_1}^2 = m_{11}^2 + \frac{1}{2}(\lambda_4 + \lambda_7 + 2\lambda_{10}'')v_2^2 \equiv m_{11}^2 + \Lambda_1 v_2^2, \quad (\text{A2})$$

$$m_{A_1}^2 = m_{11}^2 + \frac{1}{2}(\lambda_4 + \lambda_7 - 2\lambda_{10}'')v_2^2 \equiv m_{11}^2 + \bar{\Lambda}_1 v_2^2, \quad (\text{A3})$$

$$m_{H_1^\pm}^2 = m_{11}^2 + \frac{1}{2}\lambda_4 v_2^2, \quad (\text{A4})$$

$$m_{H_2}^2 = 2v_2^2 \lambda_2, \quad (\text{A5})$$

$$m_{H_3}^2 = m_{33}^2 + \frac{1}{2}(\lambda_6 + \lambda_9 + 2\lambda_{12}'')v_2^2 \equiv m_{33}^2 + \Lambda_2 v_2^2, \quad (\text{A6})$$

$$m_{A_3}^2 = m_{33}^2 + \frac{1}{2}(\lambda_6 + \lambda_9 - 2\lambda_{12}'')v_2^2 \equiv m_{33}^2 + \bar{\Lambda}_2 v_2^2, \quad (\text{A7})$$

$$m_{H_3^\pm}^2 = m_{33}^2 + \frac{1}{2}\lambda_6 v_2^2. \quad (\text{A8})$$

We have to require all these masses squared to be positive in order to have a local minimum. This is easier than finding conditions on the parameters. The value of the potential at the minimum is

$$V_{\text{FODM1}} = -\frac{m_{22}^4}{4\lambda_2}, \quad (\text{A9})$$

and this has to be compared with $V_{2\text{Inert}}$.

3. FODM2

In this case we have $v_1 \neq 0, v_2 = 0, v_3 = 0$. The minimization gives

$$v_1^2 = -\frac{m_{11}^2}{\lambda_1}, \quad (\text{A10})$$

implying $m_{11}^2 < 0$ as $\lambda_1 > 0$ from BFB. For the masses we have

$$m_{H_1}^2 = 2v_1^2 \lambda_1, \quad (\text{A11})$$

$$m_{H_2}^2 = m_{22}^2 + \frac{1}{2} (\lambda_4 + \lambda_7 + 2\lambda''_{10}) v_1^2 \equiv m_{22}^2 + \Lambda_1 v_1^2, \quad (\text{A12})$$

$$m_{A_2}^2 = m_{22}^2 + \frac{1}{2} (\lambda_4 + \lambda_7 - 2\lambda''_{10}) v_1^2 \equiv m_{22}^2 + \bar{\Lambda}_1 v_1^2, \quad (\text{A13})$$

$$m_{H_2^\pm}^2 = m_{22}^2 + \frac{1}{2} \lambda_4 v_1^2, \quad (\text{A14})$$

$$m_{H_3}^2 = m_{33}^2 + \frac{1}{2} (\lambda_5 + \lambda_8 + 2\lambda''_{11}) v_1^2 \equiv m_{33}^2 + \Lambda_3 v_1^2, \quad (\text{A15})$$

$$m_{A_3}^2 = m_{33}^2 + \frac{1}{2} (\lambda_5 + \lambda_8 - 2\lambda''_{11}) v_1^2 \equiv m_{33}^2 + \bar{\Lambda}_3 v_1^2, \quad (\text{A16})$$

$$m_{H_3^\pm}^2 = m_{33}^2 + \frac{1}{2} \lambda_5 v_1^2. \quad (\text{A17})$$

We have to require all these masses squared to be positive in order to have a local minimum. This is easier than finding conditions on the parameters. The value of the potential at the minimum is

$$V_{\text{FODM2}} = -\frac{m_{11}^4}{4\lambda_1}. \quad (\text{A18})$$

and this has to be compared with $V_{2\text{Inert}}$.

4. FODMO

In this case we have $v_1 \neq 0, v_2 \neq 0, v_3 = 0$. The minimization gives

$$v_1^2 = \frac{\lambda_2 m_{11}^2 - \Lambda_1 m_{22}^2}{\Lambda_1^2 - \lambda_1 \lambda_2}, \quad v_2^2 = \frac{\lambda_1 m_{22}^2 - \Lambda_1 m_{11}^2}{\Lambda_1^2 - \lambda_1 \lambda_2}, \quad (\text{A19})$$

requiring $v_1^2, v_2^2 > 0$. For the masses we have

$$m_{H_1}^2 = \lambda_1 v_1^2 + \lambda_2 v_2^2 - \sqrt{4\Lambda_1^2 v_1^2 v_2^2 + (\lambda_1 v_1^2 - \lambda_2 v_2^2)^2}, \quad (\text{A20})$$

$$m_{H_2}^2 = \lambda_1 v_1^2 + \lambda_2 v_2^2 + \sqrt{4\Lambda_1^2 v_1^2 v_2^2 + (\lambda_1 v_1^2 - \lambda_2 v_2^2)^2}, \quad (\text{A21})$$

$$m_{H_3}^2 = m_{33}^2 + \frac{1}{2} (\lambda_5 + \lambda_8 + 2\lambda''_{11}) v_1^2 + \frac{1}{2} (\lambda_6 + \lambda_9 + 2\lambda''_{12}) v_2^2, \quad (\text{A22})$$

$$m_{A_1}^2 = -2\lambda''_{10} (v_1^2 + v_2^2), \quad (\text{A23})$$

$$m_{A_2}^2 = m_{33}^2 + \frac{1}{2} (\lambda_5 + \lambda_8 - 2\lambda''_{11}) v_1^2 + \frac{1}{2} (\lambda_6 + \lambda_9 - 2\lambda''_{12}) v_2^2, \quad (\text{A24})$$

$$m_{H_1^\pm}^2 = -\frac{1}{2} (\lambda_7 + 2\lambda''_{10}) (v_1^2 + v_2^2), \quad (\text{A25})$$

$$m_{H_2^\pm}^2 = m_{33}^2 + \frac{1}{2} (\lambda_5 v_1^2 + \lambda_6 v_2^2). \quad (\text{A26})$$

We have to require all these masses squared to be positive in order to have a local minimum. This is easier than finding conditions on the parameters. The value of the potential at the minimum is

$$V_{\text{FODMO}} = \frac{\lambda_1 m_{22}^4 + \lambda_2 m_{11}^4 - 2m_{11}^2 m_{22}^2 \Lambda_1}{4(\Lambda_1^2 - \lambda_1 \lambda_2)}, \quad (\text{A27})$$

and this has to be compared with $V_{2\text{Inert}}$.

5. FODMO'

Let us take

$$\sqrt{r_1} = \frac{v_1}{\sqrt{2}}, \sqrt{r_2} = \frac{v_2}{\sqrt{2}}, r_3 = 0, \quad \alpha_1 = \alpha_2 = \beta_1 = \gamma = 0, \quad \beta_2 = \frac{\pi}{2}. \quad (\text{A28})$$

This is still along the neutral directions, but in comparison with FODMO corresponds to making⁷ $v_2 \rightarrow i v_2$. The stationary conditions give,

$$v_1^2 = \frac{\lambda_2 m_{11}^2 - \bar{\Lambda}_1 m_{22}^2}{\bar{\Lambda}_1^2 - \lambda_1 \lambda_2}, \quad v_2^2 = \frac{\lambda_1 m_{22}^2 - \bar{\Lambda}_1 m_{11}^2}{\bar{\Lambda}_1^2 - \lambda_1 \lambda_2}, \quad (\text{A29})$$

and

$$V_{\text{FODMO}'} = \frac{\lambda_1 m_{22}^4 + \lambda_2 m_{11}^4 - 2m_{11}^2 m_{22}^2 \bar{\Lambda}_1}{4(\bar{\Lambda}_1^2 - \lambda_1 \lambda_2)}, \quad (\text{A30})$$

where

$$\bar{\Lambda}_1 = \frac{1}{2} (\lambda_4 + \lambda_7 - 2\lambda_{10}''), \quad (\text{A31})$$

was defined before. We require that v_1^2, v_2^2 are positive and also check for the positiveness of the masses. This is not absolutely necessary, because if $V_{\text{FODMO}'} < V_{2\text{Inert}}$, even if it is a saddle-point, it indicates that there should be a minimum below and the point is not a good point. But our statement is stronger if we also identify the local minima. It should be stressed that such a minimum should exist, as our sufficient BFB conditions were checked for all cases in our numerical simulation. For the masses we have

$$m_{H_1}^2 = 2\lambda_1 v_1^2, \quad (\text{A32})$$

$$m_{H_2}^2 = 2\lambda_{10}'' v_1^2, \quad (\text{A33})$$

$$m_{H_3}^2 = \frac{1}{2} (\lambda_5 v_1^2 + \lambda_6 v_2^2 + \lambda_8 v_1^2 + \lambda_9 v_2^2 + 2\lambda_{11}' v_1^2 - 2\lambda_{12}' v_2^2 + 2m_{33}^2), \quad (\text{A34})$$

$$m_{A_1}^2 = 2\lambda_2 v_2^2, \quad (\text{A35})$$

$$m_{A_2}^2 = 2\lambda_{10}'' v_2^2, \quad (\text{A36})$$

$$m_{A_3}^2 = \frac{1}{2} (\lambda_5 v_1^2 + \lambda_6 v_2^2 + \lambda_8 v_1^2 + \lambda_9 v_2^2 - 2\lambda_{11}' v_1^2 + 2\lambda_{12}' v_2^2 + 2m_{33}^2), \quad (\text{A37})$$

$$m_{H_1^\pm}^2 = -\frac{1}{2} (\lambda_7 - 2\lambda_{10}'') (v_1^2 + v_2^2), \quad (\text{A38})$$

$$m_{H_2^\pm}^2 = \frac{1}{2} (\lambda_5 v_1^2 + \lambda_6 v_2^2 + 2m_{33}^2). \quad (\text{A39})$$

6. FOCB

Looking at the results for the new minima found by our numerical simulation, we realized that there is another particular case. It is somewhat hidden because for $v_3 = 0$ we are using too many angles. We identify a new situation, that we call FOCB, and that can be defined by

$$\sqrt{r_1} = \frac{v_1}{\sqrt{2}}, \sqrt{r_2} = \frac{v_2}{\sqrt{2}}, r_3 = 0, \quad \beta_1 = \beta_2 = \gamma = 0, \quad \alpha_1 \neq 0, \alpha_2 \neq 0. \quad (\text{A40})$$

⁷ Notice that this case is not contradiction with Eq.(3.32) of Ref. [33]. Although it looks like a particular case of sCPv, we checked explicitly by calculating the full 6×6 mass matrix for the neutral scalars that indeed that matrix separates into CP even and CP odd blocks, ensuring CP conservation.

This is, in principle, a charge breaking minimum. We get the stationary equations,

$$0 = \frac{1}{4} [4m_{11}^2 + 4\lambda_1 v_1^2 + 2\lambda_4 v_2^2 + \lambda_7 v_2^2 + 2\lambda_{10}'' v_2^2 + (\lambda_7 + 2\lambda_{10}'') v_2^2 \cos(2(\alpha_1 - \alpha_2))] \quad (\text{A41})$$

$$0 = \frac{1}{4} [4m_{22}^2 + 2\lambda_4 v_1^2 + \lambda_7 v_1^2 + 2\lambda_{10}'' v_1^2 + 4\lambda_2 v_2^2 + (\lambda_7 + 2\lambda_{10}'') v_1^2 \cos(2(\alpha_1 - \alpha_2))] \quad (\text{A42})$$

$$0 = -\frac{1}{4} (\lambda_7 + 2\lambda_{10}'') v_1^2 v_2^2 \sin(2(\alpha_1 - \alpha_2)) \quad (\text{A43})$$

$$0 = \frac{1}{4} (\lambda_7 + 2\lambda_{10}'') v_1^2 v_2^2 \sin(2(\alpha_1 - \alpha_2)) \quad (\text{A44})$$

These equations have many solutions. As we showed analytically, they are equivalent, giving the same value at the minimum. As an example, we take

$$\alpha_1 = \frac{\pi}{2}, \quad \alpha_2 = 0 \quad (\text{A45})$$

$$v_1^2 = -\frac{2(2\lambda_2 m_{11}^2 - \lambda_4 m_{22}^2)}{4\lambda_1 \lambda_2 - \lambda_4^2}, \quad v_2^2 = -\frac{2(-\lambda_4 m_{11}^2 + 2\lambda_1 m_{22}^2)}{4\lambda_1 \lambda_2 - \lambda_4^2} \quad (\text{A46})$$

and

$$V_{\text{FOCB}} = -\frac{\lambda_1 m_{22}^4 + \lambda_2 m_{11}^4 - \lambda_4 m_{11}^2 m_{22}^2}{4\lambda_1 \lambda_2 - \lambda_4^2} \quad (\text{A47})$$

To have a local minimum, we take $v_1^2, v_2^2 > 0$, as well as the squared masses to be positive,

$$m_{H_1}^2 = \frac{4\lambda_2(\lambda_4 m_{11}^2 - 2\lambda_1 m_{22}^2)}{4\lambda_1 \lambda_2 - \lambda_4^2}, \quad (\text{A48})$$

$$m_{H_2}^2 = \frac{(\lambda_7 + 2\lambda_{10}'')(\lambda_4 m_{11}^2 - 2\lambda_1 m_{22}^2)}{4\lambda_1 \lambda_2 - \lambda_4^2}, \quad (\text{A49})$$

$$m_{H_3}^2 = \frac{1}{4\lambda_1 \lambda_2 - \lambda_4^2} [4\lambda_1 \lambda_2 m_{33}^2 - 2\lambda_1 \lambda_6 m_{22}^2 - 2\lambda_1 \lambda_9 m_{22}^2 - 4\lambda_1 \lambda_{12}'' m_{22}^2 - 2\lambda_2 \lambda_5 m_{11}^2 + \lambda_4^2(-m_{33}^2) + \lambda_4 \lambda_5 m_{22}^2 + \lambda_4 \lambda_6 m_{11}^2 + \lambda_4 \lambda_9 m_{11}^2 + 2\lambda_4 \lambda_{12}'' m_{11}^2], \quad (\text{A50})$$

$$m_{A_1}^2 = \frac{(\lambda_7 - 2\lambda_{10}'')(\lambda_4 m_{11}^2 - 2\lambda_1 m_{22}^2)}{4\lambda_1 \lambda_2 - \lambda_4^2}, \quad (\text{A51})$$

$$m_{A_2}^2 = \frac{1}{4\lambda_1 \lambda_2 - \lambda_4^2} [4\lambda_1 \lambda_2 m_{33}^2 - 2\lambda_1 \lambda_6 m_{22}^2 - 2\lambda_1 \lambda_9 m_{22}^2 + 4\lambda_1 \lambda_{12}'' m_{22}^2 - 2\lambda_2 \lambda_5 m_{11}^2 + \lambda_4^2(-m_{33}^2) + \lambda_4 \lambda_5 m_{22}^2 + \lambda_4 \lambda_6 m_{11}^2 + \lambda_4 \lambda_9 m_{11}^2 - 2\lambda_4 \lambda_{12}'' m_{11}^2], \quad (\text{A52})$$

$$m_{H_1^\pm}^2 = -\frac{2\lambda_1(2\lambda_2 m_{11}^2 - \lambda_4 m_{22}^2)}{4\lambda_1 \lambda_2 - \lambda_4^2}, \quad (\text{A53})$$

$$m_{H_2^\pm}^2 = \frac{\lambda_4 \lambda_7 m_{22}^2 - 2\lambda_2 \lambda_7 m_{11}^2}{4\lambda_1 \lambda_2 - \lambda_4^2}, \quad (\text{A54})$$

$$m_{H_3^\pm}^2 = \frac{1}{4\lambda_1 \lambda_2 - \lambda_4^2} [4\lambda_1 \lambda_2 m_{33}^2 - 2\lambda_1 \lambda_6 m_{22}^2 - 2\lambda_2 \lambda_5 m_{11}^2 - 2\lambda_2 \lambda_8 m_{11}^2 + \lambda_4^2(-m_{33}^2) + \lambda_4 \lambda_5 m_{22}^2 + \lambda_4 \lambda_6 m_{11}^2 + \lambda_4 \lambda_8 m_{22}^2]. \quad (\text{A55})$$

Appendix B: Angles that minimize the angular part

We have shown that the angular part of the potential has a minimum when the functions f_7 and f_{10} in Fig. 1 are themselves extrema. We have 7 equations, 3 for f_7 and 4 for f_{10} . They are:

$$0 = \frac{\partial f_7}{\partial \alpha_+} = 2(-1 + \cos \beta) \sin(2\alpha_+), \quad (\text{B1})$$

$$0 = \frac{\partial f_7}{\partial \alpha_-} = -2(1 + \cos \beta) \sin(2\alpha_-), \quad (\text{B2})$$

$$0 = \frac{\partial f_7}{\partial \beta} = [\cos(2\alpha_+) - \cos(2\alpha_-)] \sin \beta, \quad (\text{B3})$$

and

$$0 = \frac{\partial f_{10}}{\partial \alpha_+} = -2(-1 + \cos \beta) \cos(\beta - 2\gamma) \sin(2\alpha_+) + 4 \cos(\alpha_-) \sin(\alpha_+) \sin \beta \sin(\beta - 2\gamma), \quad (\text{B4})$$

$$0 = \frac{\partial f_{10}}{\partial \alpha_-} = -2(1 + \cos \beta) \cos(\beta - 2\gamma) \sin(2\alpha_-) + 4 \cos(\alpha_+) \sin(\alpha_-) \sin \beta \sin(\beta - 2\gamma), \quad (\text{B5})$$

$$0 = -\frac{\partial f_{10}}{\partial \beta} - \frac{1}{2} \frac{\partial f_{10}}{\partial \gamma} = 4 \cos(\alpha_-) \cos(\alpha_+) \cos \beta \sin(\beta - 2\gamma) + [2 + \cos(2\alpha_-) + \cos(2\alpha_+)] \sin \beta \cos(\beta - 2\gamma), \quad (\text{B6})$$

$$0 = \frac{1}{2} \frac{\partial f_{10}}{\partial \gamma} = 4 \cos(\alpha_-) \cos(\alpha_+) \sin \beta \cos(\beta - 2\gamma) + [2 + \cos(2\alpha_-) + \cos(2\alpha_+)] \cos \beta \sin(\beta - 2\gamma) + [\cos(2\alpha_-) - \cos(2\alpha_+)] \sin(\beta - 2\gamma). \quad (\text{B7})$$

We use Eq. (B6) instead of $\partial f_{10}/\partial \beta$ because it has a simpler form. Eq. (B3) provides two cases: $\sin \beta = 0$ and $\cos(2\alpha_+) = \cos(2\alpha_-)$, which we treat separately.

1. $\sin \beta = 0; \beta = 0$

In this case, three amongst Eqs. (B1)-(B7) are automatically satisfied, while the others become:

$$\begin{aligned} 0 &= \sin(2\alpha_-), \\ 0 &= \sin(2\alpha_-) \cos(2\gamma), \\ 0 &= \cos(\alpha_-) \cos(\alpha_+) \sin(2\gamma), \\ 0 &= \cos^2(\alpha_-) \sin(2\gamma). \end{aligned} \quad (\text{B8})$$

This yields two cases. In the first

$$\beta = 0, \quad \cos \alpha_- = 0 \quad \implies \quad f_7 = 0, \quad f_{10} = 0. \quad (\text{B9})$$

In the second case

$$\beta = 0, \quad \sin \alpha_- = 0, \quad \cos(2\gamma) = \pm 1 \quad \implies \quad f_7 = 4, \quad f_{10} = \pm 4. \quad (\text{B10})$$

2. $\sin \beta = 0; \beta = \pm \pi$

In this case, three amongst Eqs. (B1)-(B7) are automatically satisfied, while the others become:

$$\begin{aligned} 0 &= \sin(2\alpha_+), \\ 0 &= \sin(2\alpha_+) \cos(2\gamma), \\ 0 &= \cos(\alpha_-) \cos(\alpha_+) \sin(2\gamma), \\ 0 &= \cos^2(\alpha_+) \sin(2\gamma). \end{aligned} \quad (\text{B11})$$

These are just Eqs. (B8) with $\alpha_- \leftrightarrow \alpha_+$. Thus, we have again two cases. In the first

$$\beta = \pi, \quad \cos \alpha_+ = 0 \quad \Longrightarrow \quad f_7 = 0, \quad f_{10} = 0. \quad (\text{B12})$$

In the second case

$$\beta = \pi, \quad \sin \alpha_+ = 0, \quad \cos(2\gamma) = \pm 1 \quad \Longrightarrow \quad f_7 = 4, \quad f_{10} = \pm 4. \quad (\text{B13})$$

3. $\sin \beta \neq 0$ and $\cos(2\alpha_+) = \cos(2\alpha_-) = 1$

When $\sin \beta \neq 0$, Eqs. (B1)-(B2) force $\sin(2\alpha_-) = 0$ and $\sin(2\alpha_+) = 0$. Since Eq. (B3) requires $\cos(2\alpha_+) = \cos(2\alpha_-)$, we are left with the case $\cos(2\alpha_+) = \cos(2\alpha_-) = 1$ treated here and with the case $\cos(2\alpha_+) = \cos(2\alpha_-) = -1$ treated in the next subsection. Under the possibilities $(\alpha_+, \alpha_-) = (0, 0), (\pi, \pi)$, Eqs. (B6)-(B7) force $\sin(2\beta - 2\gamma) = 0$. And we find:

$$(\alpha_+, \alpha_-) = (0, 0), (\pi, \pi), \quad \cos(2\beta - 2\gamma) = \pm 1 \quad \Longrightarrow \quad f_7 = 4, \quad f_{10} = \pm 4. \quad (\text{B14})$$

Similarly, under the possibilities $(\alpha_+, \alpha_-) = (0, \pi), (\pi, 0)$, Eqs. (B6)-(B7) force $\sin(2\gamma) = 0$, and we find:

$$(\alpha_+, \alpha_-) = (0, \pi), (\pi, 0), \quad \cos(2\gamma) = \pm 1 \quad \Longrightarrow \quad f_7 = 4, \quad f_{10} = \pm 4. \quad (\text{B15})$$

4. $\sin \beta \neq 0$ and $\cos(2\alpha_+) = \cos(2\alpha_-) = -1$

This is a very simple case, for all choices compatible with $\cos(2\alpha_+) = \cos(2\alpha_-) = -1$ yield:

$$\cos(2\alpha_+) = \cos(2\alpha_-) = -1 \quad \Longrightarrow \quad f_7 = 0, \quad f_{10} = 0. \quad (\text{B16})$$

-
- [1] **Planck** Collaboration, P. A. R. Ade et al., *Planck 2013 results. I. Overview of products and scientific results*, *Astron. Astrophys.* **571** (2014) A1, [[arXiv:1303.5062](#)].
- [2] F. Englert and R. Brout, *Broken Symmetry and the Mass of Gauge Vector Mesons*, *Phys. Rev. Lett.* **13** (1964) 321–323.
- [3] P. W. Higgs, *Broken Symmetries and the Masses of Gauge Bosons*, *Phys. Rev. Lett.* **13** (1964) 508–509.
- [4] **ATLAS** Collaboration, G. Aad et al., *Observation of a new particle in the search for the Standard Model Higgs boson with the ATLAS detector at the LHC*, *Phys. Lett. B* **716** (2012) 1–29, [[arXiv:1207.7214](#)].
- [5] **CMS** Collaboration, S. Chatrchyan et al., *Observation of a New Boson at a Mass of 125 GeV with the CMS Experiment at the LHC*, *Phys. Lett. B* **716** (2012) 30–61, [[arXiv:1207.7235](#)].
- [6] N. G. Deshpande and E. Ma, *Pattern of Symmetry Breaking with Two Higgs Doublets*, *Phys. Rev. D* **18** (1978) 2574.
- [7] E. Ma, *Verifiable radiative seesaw mechanism of neutrino mass and dark matter*, *Phys. Rev. D* **73** (2006) 077301, [[hep-ph/0601225](#)].
- [8] R. Barbieri, L. J. Hall, and V. S. Rychkov, *Improved naturalness with a heavy Higgs: An Alternative road to LHC physics*, *Phys. Rev. D* **74** (2006) 015007, [[hep-ph/0603188](#)].
- [9] L. Lopez Honorez, E. Nezri, J. F. Oliver, and M. H. G. Tytgat, *The Inert Doublet Model: An Archetype for Dark Matter*, *JCAP* **02** (2007) 028, [[hep-ph/0612275](#)].
- [10] A. Ilnicka, M. Krawczyk, and T. Robens, *Inert Doublet Model in light of LHC Run I and astrophysical data*, *Phys. Rev. D* **93** (2016), no. 5 055026, [[arXiv:1508.01671](#)].
- [11] A. Belyaev, G. Cacciapaglia, I. P. Ivanov, F. Rojas-Abatte, and M. Thomas, *Anatomy of the Inert Two Higgs Doublet Model in the light of the LHC and non-LHC Dark Matter Searches*, *Phys. Rev. D* **97** (2018), no. 3 035011, [[arXiv:1612.00511](#)].
- [12] J. Kalinowski, T. Robens, D. Sokolowska, and A. F. Zarnecki, *IDM Benchmarks for the LHC and Future Colliders*, *Symmetry* **13** (2021), no. 6 991, [[arXiv:2012.14818](#)].
- [13] A. Datta, N. Ganguly, N. Khan, and S. Rakshit, *Exploring collider signatures of the inert Higgs doublet model*, *Phys. Rev. D* **95** (2017), no. 1 015017, [[arXiv:1610.00648](#)].
- [14] K. P. Modak and D. Majumdar, *Confronting Galactic and Extragalactic γ -rays Observed by Fermi-lat With Annihilating Dark Matter in an Inert Higgs Doublet Model*, *Astrophys. J. Suppl.* **219** (2015), no. 2 37, [[arXiv:1502.05682](#)].
- [15] F. S. Queiroz and C. E. Yaguna, *The CTA aims at the Inert Doublet Model*, *JCAP* **02** (2016) 038, [[arXiv:1511.05967](#)].
- [16] C. Garcia-Cely, M. Gustafsson, and A. Ibarra, *Probing the Inert Doublet Dark Matter Model with Cherenkov Telescopes*, *JCAP* **02** (2016) 043, [[arXiv:1512.02801](#)].

- [17] E. Nezri, M. H. G. Tytgat, and G. Vertongen, *e^+ and anti- p from inert doublet model dark matter*, *JCAP* **04** (2009) 014, [[arXiv:0901.2556](#)].
- [18] P. Agrawal, E. M. Dolle, and C. A. Krenke, *Signals of Inert Doublet Dark Matter in Neutrino Telescopes*, *Phys. Rev. D* **79** (2009) 015015, [[arXiv:0811.1798](#)].
- [19] S. Andreas, M. H. G. Tytgat, and Q. Swillens, *Neutrinos from Inert Doublet Dark Matter*, *JCAP* **04** (2009) 004, [[arXiv:0901.1750](#)].
- [20] C. Boehm, P. Fayet, and J. Silk, *Light and heavy dark matter particles*, *Phys. Rev. D* **69** (2004) 101302, [[hep-ph/0311143](#)].
- [21] K. M. Zurek, *Multi-Component Dark Matter*, *Phys. Rev. D* **79** (2009) 115002, [[arXiv:0811.4429](#)].
- [22] B. Batell, M. Pospelov, and A. Ritz, *Direct Detection of Multi-component Secluded WIMPs*, *Phys. Rev. D* **79** (2009) 115019, [[arXiv:0903.3396](#)].
- [23] S. Profumo, K. Sigurdson, and L. Ubaldi, *Can we discover multi-component WIMP dark matter?*, *JCAP* **12** (2009) 016, [[arXiv:0907.4374](#)].
- [24] S. Mizuta and M. Yamaguchi, *Coannihilation effects and relic abundance of Higgsino dominant LSP(s)*, *Phys. Lett. B* **298** (1993) 120–126, [[hep-ph/9208251](#)].
- [25] J. R. Ellis, T. Falk, and K. A. Olive, *Neutralino - Stau coannihilation and the cosmological upper limit on the mass of the lightest supersymmetric particle*, *Phys. Lett. B* **444** (1998) 367–372, [[hep-ph/9810360](#)].
- [26] Z.-P. Liu, Y.-L. Wu, and Y.-F. Zhou, *Enhancement of dark matter relic density from the late time dark matter conversions*, *Eur. Phys. J. C* **71** (2011) 1749, [[arXiv:1101.4148](#)].
- [27] F. D’Eramo and J. Thaler, *Semi-annihilation of Dark Matter*, *JHEP* **06** (2010) 109, [[arXiv:1003.5912](#)].
- [28] G. Belanger, K. Kannike, A. Pukhov, and M. Raidal, *Impact of semi-annihilations on dark matter phenomenology - an example of Z_N symmetric scalar dark matter*, *JCAP* **04** (2012) 010, [[arXiv:1202.2962](#)].
- [29] G. Belanger, A. Mjallal, and A. Pukhov, *Two dark matter candidates: The case of inert doublet and singlet scalars*, *Phys. Rev. D* **105** (2022), no. 3 035018, [[arXiv:2108.08061](#)].
- [30] G. Belanger and J.-C. Park, *Assisted freeze-out*, *JCAP* **03** (2012) 038, [[arXiv:1112.4491](#)].
- [31] M. Aoki, M. Duerr, J. Kubo, and H. Takano, *Multi-Component Dark Matter Systems and Their Observation Prospects*, *Phys. Rev. D* **86** (2012) 076015, [[arXiv:1207.3318](#)].
- [32] S. Bhattacharya, P. Poulose, and P. Ghosh, *Multipartite Interacting Scalar Dark Matter in the light of updated LUX data*, *JCAP* **04** (2017) 043, [[arXiv:1607.08461](#)].
- [33] J. Hernandez-Sanchez, V. Keus, S. Moretti, D. Rojas-Ciofalo, and D. Sokolowska, *Complementary Probes of Two-component Dark Matter*, [arXiv:2012.11621](#).
- [34] S. Bhattacharya, P. Ghosh, J. Lahiri, and B. Mukhopadhyaya, *Distinguishing two dark matter component particles at e^+e^- colliders*, *JHEP* **12** (2022) 049, [[arXiv:2202.12097](#)].
- [35] S. Bhattacharya, P. Ghosh, J. Lahiri, and B. Mukhopadhyaya, *Mono- X signal and two component dark matter: New distinction criteria*, *Phys. Rev. D* **108** (2023), no. 11 L111703, [[arXiv:2211.10749](#)].
- [36] R. Boto, J. C. Romão, and J. a. P. Silva, *Bounded from below conditions on a class of symmetry constrained 3HDM*, *Phys. Rev. D* **106** (2022), no. 11 115010, [[arXiv:2208.01068](#)].
- [37] J. Hernandez-Sanchez, V. Keus, S. Moretti, and D. Sokolowska, *Complementary collider and astrophysical probes of multi-component Dark Matter*, *JHEP* **03** (2023) 045, [[arXiv:2202.10514](#)].
- [38] I. P. Ivanov, V. Keus, and E. Vdovin, *Abelian symmetries in multi-Higgs-doublet models*, *J. Phys. A* **45** (2012) 215201, [[arXiv:1112.1660](#)].
- [39] V. Keus, S. F. King, and S. Moretti, *Three-Higgs-doublet models: symmetries, potentials and Higgs boson masses*, *JHEP* **01** (2014) 052, [[arXiv:1310.8253](#)].
- [40] S. Weinberg, *Gauge Theory of CP Violation*, *Phys. Rev. Lett.* **37** (1976) 657.
- [41] B. Grzadkowski, O. M. Ogreid, and P. Osland, *Natural Multi-Higgs Model with Dark Matter and CP Violation*, *Phys. Rev. D* **80** (2009) 055013, [[arXiv:0904.2173](#)].
- [42] F. S. Faro and I. P. Ivanov, *Boundedness from below in the $U(1) \times U(1)$ three-Higgs-doublet model*, *Phys. Rev. D* **100** (2019), no. 3 035038, [[arXiv:1907.01963](#)].
- [43] S. Moretti and K. Yagyu, *Constraints on Parameter Space from Perturbative Unitarity in Models with Three Scalar Doublets*, *Phys. Rev. D* **91** (2015) 055022, [[arXiv:1501.06544](#)].
- [44] M. P. Bento, J. C. Romão, and J. a. P. Silva, *Unitarity bounds for all symmetry-constrained 3HDMs*, *JHEP* **08** (2022) 273, [[arXiv:2204.13130](#)].
- [45] I. Bree, S. Carrolo, J. C. Romao, and J. P. Silva, *A viable A_4 3HDM theory of quark mass matrices*, *Eur. Phys. J. C* **83** (2023), no. 4 292, [[arXiv:2301.04676](#)].
- [46] F. James and M. Roos, *Minuit: A System for Function Minimization and Analysis of the Parameter Errors and Correlations*, *Comput. Phys. Commun.* **10** (1975) 343–367.
- [47] A. Pierce and J. Thaler, *Natural Dark Matter from an Unnatural Higgs Boson and New Colored Particles at the TeV Scale*, *JHEP* **08** (2007) 026, [[hep-ph/0703056](#)].
- [48] D. Fontes and J. C. Romão, *FeynMaster: a plethora of Feynman tools*, *Comput. Phys. Commun.* **256** (2020) 107311, [[arXiv:1909.05876](#)].
- [49] D. Fontes and J. C. Romão, *Renormalization of the C2HDM with FeynMaster 2*, *JHEP* **06** (2021) 016, [[arXiv:2103.06281](#)]. [Erratum: *JHEP* **12**, 005 (2021)].
- [50] A. Alloul, N. D. Christensen, C. Degrande, C. Duhr, and B. Fuks, *FeynRules 2.0 - A complete toolbox for tree-level phenomenology*, *Comput. Phys. Commun.* **185** (2014) 2250–2300, [[arXiv:1310.1921](#)].
- [51] G. Alguero, G. Belanger, F. Boudjema, S. Chakraborti, A. Goudelis, S. Kraml, A. Mjallal, and A. Pukhov,

- micrOMEGAs 6.0: N-component dark matter*, *Comput. Phys. Commun.* **299** (2024) 109133, [[arXiv:2312.14894](#)].
- [52] **Gfitter Group** Collaboration, M. Baak, J. Cúth, J. Haller, A. Hoecker, R. Kogler, K. Mönig, M. Schott, and J. Stelzer, *The global electroweak fit at NNLO and prospects for the LHC and ILC*, *Eur. Phys. J. C* **74** (2014) 3046, [[arXiv:1407.3792](#)].
- [53] W. Grimus, L. Lavoura, O. M. Ogreid, and P. Osland, *The Oblique parameters in multi-Higgs-doublet models*, *Nucl. Phys. B* **801** (2008) 81–96, [[arXiv:0802.4353](#)].
- [54] **ATLAS** Collaboration, G. Aad et al., *A detailed map of Higgs boson interactions by the ATLAS experiment ten years after the discovery*, *Nature* **607** (2022), no. 7917 52–59, [[arXiv:2207.00092](#)]. [Erratum: *Nature* 612, E24 (2022)].
- [55] M. Spira, *HIGLU: A program for the calculation of the total Higgs production cross-section at hadron colliders via gluon fusion including QCD corrections*, [hep-ph/9510347](#).
- [56] **LHC Higgs Cross Section Working Group** Collaboration, D. de Florian et al., *Handbook of LHC Higgs Cross Sections: 4. Deciphering the Nature of the Higgs Sector*, [arXiv:1610.07922](#).
- [57] **CMS** Collaboration, A. M. Sirunyan et al., *Measurements of the Higgs boson width and anomalous HVV couplings from on-shell and off-shell production in the four-lepton final state*, *Phys. Rev. D* **99** (2019), no. 11 112003, [[arXiv:1901.00174](#)].
- [58] E. Lundstrom, M. Gustafsson, and J. Edsjo, *The Inert Doublet Model and LEP II Limits*, *Phys. Rev. D* **79** (2009) 035013, [[arXiv:0810.3924](#)].
- [59] J. Heisig, S. Kraml, and A. Lessa, *Constraining new physics with searches for long-lived particles: Implementation into SModelS*, *Phys. Lett. B* **788** (2019) 87–95, [[arXiv:1808.05229](#)].
- [60] H. Bahl, T. Biekötter, S. Heinemeyer, C. Li, S. Paasch, G. Weiglein, and J. Wittbrodt, *HiggsTools: BSM scalar phenomenology with new versions of HiggsBounds and HiggsSignals*, *Comput. Phys. Commun.* **291** (2023) 108803, [[arXiv:2210.09332](#)].
- [61] **Planck** Collaboration, N. Aghanim et al., *Planck 2018 results. VI. Cosmological parameters*, *Astron. Astrophys.* **641** (2020) A6, [[arXiv:1807.06209](#)]. [Erratum: *Astron. Astrophys.* 652, C4 (2021)].
- [62] S. Banerjee, F. Boudjema, N. Chakrabarty, G. Chalons, and H. Sun, *Relic density of dark matter in the inert doublet model beyond leading order: The heavy mass case*, *Phys. Rev. D* **100** (2019), no. 9 095024, [[arXiv:1906.11269](#)].
- [63] S. Banerjee, F. Boudjema, N. Chakrabarty, and H. Sun, *Relic density of dark matter in the inert doublet model beyond leading order for the low mass region: 4. The Higgs resonance region*, *Phys. Rev. D* **104** (2021) 075005, [[arXiv:2101.02170](#)].
- [64] **LZ** Collaboration, J. Aalbers et al., *First Dark Matter Search Results from the LUX-ZEPLIN (LZ) Experiment*, *Phys. Rev. Lett.* **131** (2023), no. 4 041002, [[arXiv:2207.03764](#)].
- [65] G. Bélanger, K. Kannike, A. Pukhov, and M. Raidal, *Minimal semi-annihilating \mathbb{Z}_N scalar dark matter*, *JCAP* **06** (2014) 021, [[arXiv:1403.4960](#)].
- [66] **Fermi-LAT** Collaboration, M. Ackermann et al., *Searching for Dark Matter Annihilation from Milky Way Dwarf Spheroidal Galaxies with Six Years of Fermi Large Area Telescope Data*, *Phys. Rev. Lett.* **115** (2015), no. 23 231301, [[arXiv:1503.02641](#)].
- [67] **AMS** Collaboration, M. Aguilar et al., *Antiproton Flux, Antiproton-to-Proton Flux Ratio, and Properties of Elementary Particle Fluxes in Primary Cosmic Rays Measured with the Alpha Magnetic Spectrometer on the International Space Station*, *Phys. Rev. Lett.* **117** (2016), no. 9 091103.
- [68] **AMS** Collaboration, M. Aguilar et al., *Precision Measurement of the Boron to Carbon Flux Ratio in Cosmic Rays from 1.9 GV to 2.6 TV with the Alpha Magnetic Spectrometer on the International Space Station*, *Phys. Rev. Lett.* **117** (2016), no. 23 231102.
- [69] A. Reinert and M. W. Winkler, *A Precision Search for WIMPs with Charged Cosmic Rays*, *JCAP* **01** (2018) 055, [[arXiv:1712.00002](#)].
- [70] **H.E.S.S.** Collaboration, H. Abdalla et al., *Search for Dark Matter Annihilation Signals in the H.E.S.S. Inner Galaxy Survey*, *Phys. Rev. Lett.* **129** (2022), no. 11 111101, [[arXiv:2207.10471](#)].
- [71] **XENON** Collaboration, E. Aprile et al., *Dark Matter Search Results from a One Ton-Year Exposure of XENON1T*, *Phys. Rev. Lett.* **121** (2018), no. 11 111302, [[arXiv:1805.12562](#)].
- [72] **DARWIN** Collaboration, J. Aalbers et al., *DARWIN: towards the ultimate dark matter detector*, *JCAP* **11** (2016) 017, [[arXiv:1606.07001](#)].
- [73] C. A. J. O’Hare, *New Definition of the Neutrino Floor for Direct Dark Matter Searches*, *Phys. Rev. Lett.* **127** (2021), no. 25 251802, [[arXiv:2109.03116](#)].
- [74] M. Krawczyk, M. Matej, D. Sokolowska, and B. Świeżewska, *The Universe in the Light of LHC*, *Acta Phys. Polon. B* **46** (2015), no. 1 169–179, [[arXiv:1501.04529](#)].
- [75] M. Krawczyk, D. Sokolowska, P. Swaczyna, and B. Świeżewska, *Constraining Inert Dark Matter by $R_{\gamma\gamma}$ and WMAP data*, *JHEP* **09** (2013) 055, [[arXiv:1305.6266](#)].
- [76] **ATLAS** Collaboration, G. Aad et al., *A search for the $Z\gamma$ decay mode of the Higgs boson in pp collisions at $\sqrt{s} = 13$ TeV with the ATLAS detector*, *Phys. Lett. B* **809** (2020) 135754, [[arXiv:2005.05382](#)].
- [77] **ATLAS, CMS** Collaboration, G. Aad et al., *Evidence for the Higgs Boson Decay to a Z Boson and a Photon at the LHC*, *Phys. Rev. Lett.* **132** (2024), no. 2 021803, [[arXiv:2309.03501](#)].
- [78] **CMS** Collaboration, A. Tumasyan et al., *Search for Higgs boson decays to a Z boson and a photon in proton-proton collisions at $\sqrt{s} = 13$ TeV*, *JHEP* **05** (2023) 233, [[arXiv:2204.12945](#)].
- [79] R. Boto, D. Das, J. C. Romao, I. Saha, and J. P. Silva, *New physics interpretations for nonstandard values of $h \rightarrow Z\gamma$* ,

